Nanoscale

Accepted Manuscript

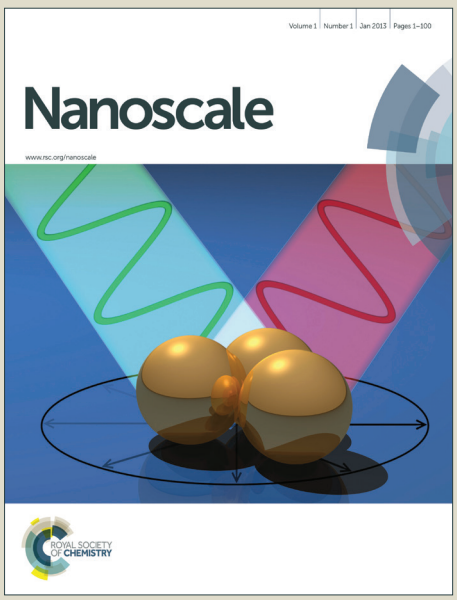

ROYAL SOCIETY OF CHEMISTRY

www.rsc.org/nanoscale

Nanoscale

REVIEW

Self-assembled and Pyrolyzed Carbon Aerogels: an Overview on Preparation Mechanisms, Properties and Applications

Received 00th January 20xx,
Accepted 00th January 20xx

DOI: 10.1039/x0xx00000x

www.rsc.org/

Ahmad Allahbakhsh and Ahmad Reza Bahramian*

An overview of the synthesis conditions and mechanisms for the fabrication of different types of carbon aerogels, as well as structural and functional properties of these materials, is presented here. In this overview, carbon aerogels are classified into three major categories: (i) conventional pyrolyzed organic-based carbon aerogels, which are products of the pyrolysis process of organic aerogels; (ii) self-assembled carbon aerogels, which are products of a reduction process; and (iii) nanocomposite carbon aerogels. Synthesis mechanisms for the sol-gel process of organic aerogels are covered using different suggested mechanisms in the literature. Moreover, the overall fabrication process of self-assembled carbon aerogels (graphene and carbon nanotubes aerogels) is covered and the suggested mechanism for the gelation process of self-assembled carbon aerogels during the reduction process is investigated using reported mechanisms. Structural performance and functional properties (electrochemical and thermal properties) of different types of carbon aerogels are covered in details. Moreover, different structural features of carbon aerogels and the influences of synthesis conditions on these structural characteristics are assessed and compared. Based on literature results covered in this review paper, carbon aerogels are perfect candidates for the fabrication of ultra-low density supercapacitors, as well as thermal insulating materials.

1. Introduction

In classic categorization of aerogel materials, carbon aerogels are defined as a class of porous materials with very low densities, which are the product of the pyrolysis process of an organic aerogel. With enormous developments in the field of graphene- and carbon nanotubes-based aerogels during last decade, however, the word "carbon aerogel" cannot be just dedicated to a specific class of conventional pyrolyzed organic-derived aerogels anymore. Interestingly, new members of this category (e.g. graphene- and carbon nanotubes-based aerogels) presented even more fascinating properties and structural characteristics than the old ones.

The idea of carbon aerogels was first developed by Pekala and coworkers during 1990s, which presented a method for the fabrication of carbon aerogels from pyrolysis process of organic precursors.[1, 2] Pekala's porous material attracted a great interest and the number of articles concerning carbon aerogels increased noticeably in the literature. Synthesis conditions, functional properties and structural tailoring of carbon aerogels were the subject of many articles and review papers during past years, and huge developments have been made in this way.[3-5] The structure of carbon aerogels, fabricated from pyrolysis process of organic aerogels, is mostly amorphous and hence, most of the functional properties of these materials are depended on the efficiency of sol-gel polymerization as well as the pyrolysis process. However, structurally ordered carbon aerogels became accessible by introduction of carbon nanotubes hydrogels and aerogels.[6, 7] Moreover, fabrication of graphene aerogels during last decade[8-10], expanded the area of carbon aerogels from almost fully amorphous materials to ordered ones.

The objective of this review paper, therefore, is to give an overview of the published works in the carbon aerogels category as a whole. This review can be considered as a starting point for those interested in different types of carbon aerogels, and can provide initiating information regarding synthesis processes, structural characteristics and properties of these materials. The opening section of this review is dedicated to the synthesis conditions and mechanisms for the fabrication of different types of carbon aerogels. A brief description of the fabrication steps and mechanisms is presented for each type of carbon aerogels in section 2. The nature of differences between different types of carbon aerogels is in structural characteristics. Therefore, structural characteristics of different carbon aerogels are covered and compared in section 3. The last section of this review paper is about the functional properties and potential application fields for carbon aerogels. The authors have restricted details in this part of the review to electrochemical and thermal properties of different carbon aerogel types, as these two can be considered as the most interested potential applications for these materials.

Department of Polymer Engineering, Faculty of Chemical Engineering, Tarbiat Modares University, P.O. 14115-114, Tehran, Iran. E-mail: abahramian@modares.ac.ir.

2. Preparation methods and mechanisms

Based on the preparation method, carbon aerogels can be classified into three major categories: (i) conventional organic-based pyrolyzed carbon aerogels, (ii) self-assembled carbon aerogels, and (iii) nanocomposite carbon aerogels. Final performance and structural characteristics of carbon aerogels differ by the preparation mechanism. The total surface area, pore volume, meso- and micro-porosity, and bulk density are the main characteristics which depend strongly on the aerogel preparation method. Preparation methods used throughout the literature for the fabrication of pyrolyzed, self-assembled and nanocomposite-based carbon aerogels as well as suggested mechanisms for each method are covered briefly in this section.

2.1. Conventional pyrolyzed carbon aerogels

The pyrolysis of organic aerogels is the well-known method for the preparation of carbon aerogels. In this method, an organic precursor aerogel is pyrolyzed in a typical thermal treatment program. Different types of organic sources can be used for the synthesis of organic precursors. Resorcinol/formaldehyde [11], resorcinol/furfural [12], cresol/formaldehyde [13], phenolic novolak/furfural [14], novolak/methyl ethyl ketone [15, 16], novolak/hexamethylenetetramine [17], phenolic resoles/methylolated melamine [18], phenol/formaldehyde [19], phenol/furfural [20], polyurethane based organic aerogels [21], and poly(vinyl chloride) based [22] organic aerogels are some of the most studied organic systems, used as the precursor for the preparation of carbon aerogels. Resorcinol/formaldehyde (RF), however, can be considered as the most interested organic precursor system, which mostly is prepared through polycondensation sol–gel polymerization of resorcinol and formaldehyde, followed by a drying method.[1, 23-26]

In a typical sol-gel process of a RF system, a given molar ratio of sodium carbonate as a catalyst (C) is mixed with an aqueous solution of resorcinol (R) and formaldehyde (F) as reactants, and deionized water (W) as solvent. Then, the solution is remained at temperatures in the range of 85–95 °C for gelling and curing in a glass container. Upon completion of the cure cycle, the prepared RF gel should be placed in an agitated acetone bath for solvent exchange process. The acetone-filled gel can then be dried using a drying method, resulting in an organic aerogel. A pyrolysis heating program should next be used to convert the organic precursor to the carbon aerogel. The described above method, known as Pekala's route, is the most common procedure for the preparation of carbon aerogels.[26-30]

The polymerization mechanism of RF system is reported to include two main steps: (i) formation of resorcinol anions by hydrogen abstraction (enhanced by OH^-) and formaldehyde addition to obtain hydroxymethyl derivatives; and (ii) condensation of the hydroxymethyl derivatives and cluster growth (catalyzed by H^+).[31] Afterward, the growing clusters suddenly become unstable and gelation occurs due to spinodal decomposition.[31] The concentration of used catalyst has a clear effect on the stability of clusters and gelation process. High catalyst concentrations in an RF sol-gel process leads to the formation of highly branched cross-linked clusters, which are less stable towards spinodal decomposition and as a result smaller and more interconnected polymer particles form.[31] A schematic diagram of described mechanism and structure of expected cross-linked polymer network of RS system is presented in **Figure 1**.

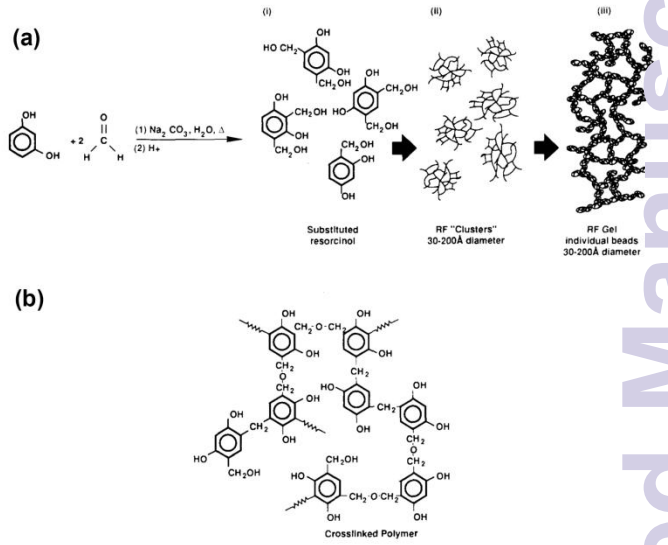

Figure 1. A schematic diagram of (a) resorcinol/formaldehyde polymerization process and (b) the structure of the crosslinked polymer network (Reproduced with permission.[32] Copyright 1990, Elsevier B.V.).

The sol-gel processes conditions, including resorcinol to the formaldehyde molar ratio (R/F), resorcinol to the catalyst molar ratio (R/C), and resorcinol to water molar ratio (R/W) dictate the final structure of carbon aerogels.[33, 34] Moreover, selected drying procedure for the preparation of RF aerogels also affects the final structural performance of carbon aerogels.[35] Supercritical drying, freeze drying, and evaporative drying are three drying methods for the preparation of organic precursor aerogels.[33, 36, 37] Due to the capillary forces which arise within the pores throughout evaporative drying, this method is not prevalent for the drying of organic aerogels.[35] However, evaporative drying is suitable when a dense carbon aerogel is needed or when the control on the pore size is essential.[35]

Highest pore volume and the widest texture range are accessible via supercritical drying, as the original pure texture of carbon aerogels can be saved through this method.[35] In a typical CO_2 supercritical drying procedure, the water in the pores is first replaced by acetone to reduce the drying time. The acetone is then replaced by liquid CO_2 in a reactor under pressure. Finally, the temperature is raised to the critical point of CO_2 under pressure to remove CO_2.[38-40] Some structural shrinkages are unavoidable in this drying process due to residual solvents, which remain after exchange steps and can lead to residual surface tensions.[35] These tensions are more when CO_2 supercritical drying procedure is used for the low-density carbon aerogels. Mentioned shrinkage can only be completely avoided with high R/C and R/W ratios. Moreover,

prolonged solvent exchange steps can reduce shrinkage when R/C ratio is low.[35]

The monolith and low density aerogels are very difficult to obtain by freeze-drying, because of the appearance of huge channels of ice crystal growth during drying process. However, freeze-drying is more economical and easier to operate than supercritical drying method.[5, 38] During this drying procedure, the wet gel is frozen by immersing its container into the liquid nitrogen to convert water to ice. Afterward, the frozen aqueous solution is removed from the gel by sublimation under low pressures, which this pressure must be lower than the vapor pressure of the frozen solvent at the set temperature. Finally, the residual adsorbed solvent on the solid surface is converted to vapor and removed from the material under very low pressure. The rate of these three steps, which known as freezing, sublimation, and desorption, influences the final pore texture of the aerogel.[5, 41-43]

Catalyst type is another factor, which can affect the final characteristics of carbon aerogels. The size, shape and connectivity of the primary particles strongly depend on the catalyst type and amount used in sol-gel process. Therefore, different types of basic and acid catalysts have been used in the literature to control the structural performance of carbon aerogels. Basic catalysts, however, are more frequent due to their ability to form higher crosslink densities.[44]

Among these catalysts, sodium carbonate is the most interested catalyst for RF system, because of the noticeable structural controllability that is accessible via this type of catalyst. RF organic aerogels synthesized in the presence of sodium carbonate are smaller in particle size when the concentration of catalyst is high, as clusters are less stable with high sodium carbonate concentrations. Formation of hydroxymethyl-derivatives increases at the higher OH^-/H^+ ratio and consequently, high catalytic concentrations results in highly branched clusters with less stability towards spinodal decomposition.[31, 45] In addition to widely used sodium carbonate (Na_2CO_3) [46, 47], potassium carbonate (K_2CO_3) [46], potassium hydrogencarbonate ($KHCO_3$) [46], sodium hydrogencarbonate ($NaHCO_3$) [46], hexamethylenetetramine (HMTA) [12, 48], magnesium acetate [47], hydrogen chloride (HCl) [49], acetic acid [50], *para*-toluenesulfonic acid (PTSA) [51], and oxalic acid (OA) [51] are catalysts used throughout the literature for the fabrication of RF organic aerogels. A comparison between structural characteristics of carbon aerogels prepared different basic and acid catalysts is presented in **Table 1**.

The final step toward preparation of carbon aerogels fro organic precursors is the pyrolysis process. In this step, organi aerogel should be pyrolyzed using a heating program t remove oxygen- and hydrogen-containing groups. Hydrogen elimination during the pyrolysis process leads to the formatio of bi-dimensional nanolayers and as a result, a highly interconnected network structure.[5] A typical pyrolysis progra for the fabrication of carbon aerogel from organic precursors is presented in **Figure 2**. The pyrolysis temperature has a direct impact on the final properties of carbon aerogels. Pore volum of carbon gels increases with increasing the temperature i this process. As the carbonization temperature increases, modification in the porous structure of the gel (mor micropores) is expected, as volatile matters release more a higher temperatures.[13, 31, 52]

2.2. Self-assembled carbon aerogels

Based on the used source for the self-assembly of carbon aerogels, one can classify self-assembled carbon aerogels int carbon nanotubes aerogels (CNTAs) and graphene aerogels (GAs). However, Wu *et al.* [53] reported an interesting metho for the assembly of carbonaceous hydrogels and aerogels via a one-pot hydrothermal reaction of watermelon. The reported method can be considered as a fascinating procedure for th green fabrication of carbon aerogels. Nevertheless, here w focus on self-assembly techniques for the fabrication of carbo aerogels from carbon nanotubes (CNTs) and graphene oxide (GO) as the starting materials. Final properties and structure o self-assembled carbon aerogels strongly depend on the assembly process and binding conditions. The finishin performance of aerogels also depends on using or eliminating a binder material. Therefore, a clear vision over the self assembly process conditions seems essential to understa the final performance of this class of carbon aerogels, and to control structural characteristics.

Table 1. Structural characteristics of carbon aerogels prepared using different catalyst types

Organic system	Organic ratio	Catalyst type	Resorcinol/catalyst ratio	Density (g/cm^3)	S_{BET} (m^2/g)	V_{micro} (cm^3/g)	V_{meso} (cm^3/g)	Reference
Resorcinol/formaldehyde	0.5	Na2CO3	50	--	720	0.29	0.39-1.30	46
Resorcinol/formaldehyde	0.5	K2CO3	50	--	690	0.27	0.42	46
Resorcinol/formaldehyde	0.5	KHCO3	50	--	770	0.31	0.70	46
Resorcinol/formaldehyde	0.5	NaHCO3	50	--	770	0.30	0.79	46
Resorcinol/formaldehyde	0.4	magnesium acetate	50	--	723	0.14	--	47
Resorcinol/formaldehyde	0.5	PTSA	8000	1.04	751	0.28	0.33	51
Resorcinol/formaldehyde	0.5	OA	800	0.86	740	0.32	0.70	51
Resorcinol/furfural	0.5	HMTA	50	0.18	663	0.24	0.29	12

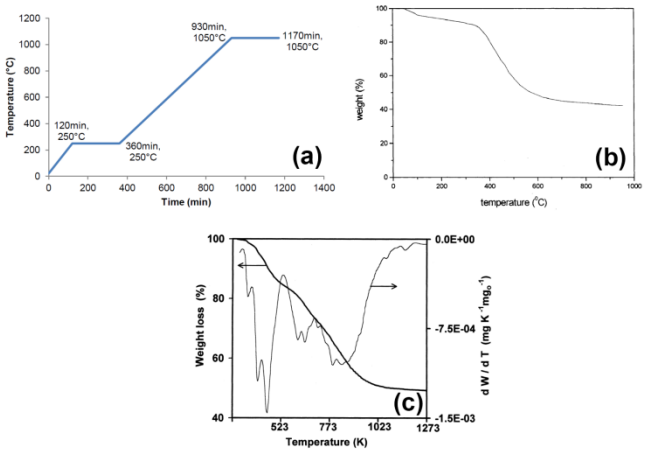

Figure 2. A typical heating program for the carbonization of an cresol/formaldehyde aerogel (a) and a typical thermorgravimetric analysis (TGA) results for the same aerogel (b) (Reproduced with permission.[13] Copyright 2001, Elsevier B.V.), as well as a typical TGA curve of RF aerogels (c) (Reproduced with permission.[54] Copyright 1999, Elsevier B.V.).

CNTAs are always fabricated from a stable homogenous suspension of fully dispersed CNTs. Therefore, preparation of such a suspension is the first step toward the assembly process. CNTs cannot be suspended in water or polar solvents in their pure form, despite the presence of some amount of functional groups or dispersant agents on their surface region.[6] Presence of such molecules and their molecular structure affects both dispersion-ability and self-assembly process of nanotubes. Oxidation process is a simple and efficient method for the preparation of stable exfoliated graphite-based nanomaterials suspensions without using any surfactant or stabilizing agents.[6] Oxidized-CNTs readily can be dispersed in water to form suspension, when they acquire negative surface charge.[6] Therefore, sonication of oxidized CNTs suspension results in a stable exfoliated suspension, which can be used for the self-assembly purpose.

In addition to the oxidation process, using different types of dispersant agents is reported to be a promising method for the preparation of a stable CNTs suspension. Dispersant agents should have appropriate active sites to incorporate in the gelation process. Chen *et al.* [7] used ferrocene-grafted poly(p-phenyleneethynylene) (PPE) as a dispersant agent for the fabrication of CNTs organogels from single-walled carbon nanotubes (SWNTs). They show that presence of aromatic functional groups, which can form π–π interactions between SWNTs surfaces, result in a cross-linked 3D nanotube network in the solution. Chemical structure of PPE as well as proposed mechanism for the formation of 3D network of SWNTs by cross-linking CNTs via π–π interactions between ferrocenyl groups of SWNTs and the neighboring CNTs surfaces, are presented in **Figure 3**.

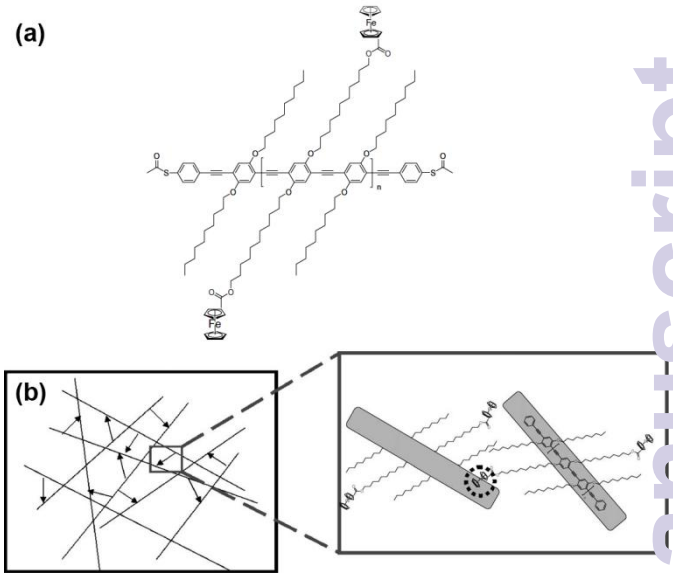

Figure 3. Chemical structure (a) and crosslinking mechanism (b) of SWNTs organiz through π–π interactions of SWNTs ferrocenyl groups and neighbor CNTs surfa (Reproduced with permission.[7] Copyright 2006, Elsevier B.V.).

Sodium dodecylbenzene sulfonate (SDBS) is also reported a an efficient surfactant for the preparation of graphite-based nanomaterials stable dispersions.[55] Bryning *et al.* [55] stated tha the sufficient surfactant/CNT weight ratio was 5:1 and that higher CNT concentrations result in aggregation. Chitosan also reported as an efficient sustainable dispersion agent fo CNTs, which provides homogeneous suspensions.[5] Conjugated-block-copolymers are another class of dispersants which contain conjugated-polymer-blocks as well as non conjugated ones, as shown in **Figure 4**. The conjugated polymer blocks can establish π–π interactions with CNT walls while the non-conjugated polymer blocks provide the de bundled CNTs with a good solubility and stability in a wid range of organic solvents.[57, 58]

Once a stable dispersion of CNTs is prepared, one can fabric e CNTAs via either physical or chemical gelation of CNTs suspension, followed by an appropriate drying process. Physical gelation of oxidized-CNTs can be achieved in CNT concentrations ≥ 0.3 wt. %.[6] In addition, In the case of oxidized multi-walled nanotubes (MWNTs), a viscoelastic gel is expected at concentrations around 8 wt. %.[6] Bryning *et al.* [5 poured SDBS-stabilized-CNTs suspension into a cylindrical mold and prepared a CNTAs through overnight physica gelation followed by a freeze drying step. They also prepared polyvinyl alcohol (PVA) reinforced aerogels through solution diffusion of PVA chains into the CNTs 3D network after fabrication of CNTs hydrogels.[55]

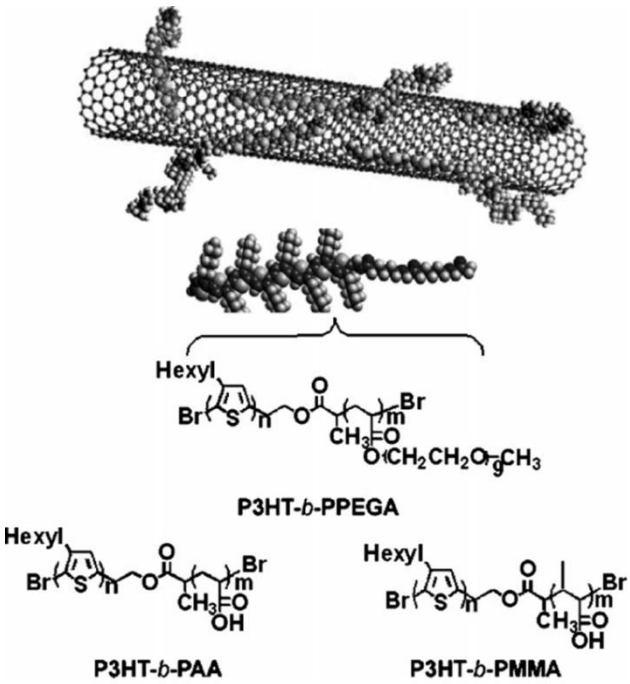

Figure 4. Dispersion mechanisms of CNTs via conjugated poly(acrylic acid) (PAA) and poly(methyl methacrylate) (PMMA) block copolymers; in this figure P3HT-*b*-PMMA: poly(3-hexylthiophene)- b-poly(methyl methacrylate), P3HT-*b*-PAA: poly(3-hexylthiophene)-b-poly(acrylic acid), P3HT-*b*-PPEGA: poly(3-hexylthiophene)-b-poly(ethylene glycol) methyl ether acrylate (Reproduced with permission.[58] Copyright 2009, WILEY-VCH Verlag GmbH & Co).

Chemical crosslinking of dispersed CNTs suspension involves using a binder material and/or dispersant agent groups to form a 3D CNTs network. In this method, assembled-aerogel is more consolidated and performs enhanced structural characteristics. PPE is a dispersant agent with the capability to form 3D CNTs network through π–π interactions between PPE aromatic functional groups and SWNT surface (see Figure 4). Kohlmeyer *et al.* [59] used this chemical crosslinker besides ferrocene-grafted poly((p-phenyleneethynylene)-alt-(2,5-thienyleneethynylene)) (Fc-PPETE) to form a set of CNTAs. They used different CNTs:chemical crosslinker mass ratios to investigate the influences of crosslinkers amounts on the structure of aerogels. They reported that it took about one week to form CNTs hydrogels from CNTs suspensions, and they used CO_2 supercritical drying method to prepare CNTAs from solvent-exchanged hydrogels.[7, 59] They also annealed prepared CNTAs to investigate effects of annealing conditions on electrical and mechanical performance of final aerogels.

Stabilized suspension of dispersed CNTs and chitosan can also be converted into a CNTA using ice segregation induced self-assembly method, as reported by Gutierrez and coworkers.[56] In their study, functionalized MWNTs were stabilized using chitosan and then, the suspension was maintained at a constant temperature around –196 °C and at ambient pressure. Prepared hydrogel was freeze-dried to form a 3D network of MWNTs, crosslinked via chitosan macromolecules.[56] They also show that MWNTs content as well as freezing direction through hydrogel fabrication, can affect morphology and conductivity of final CNTAs.

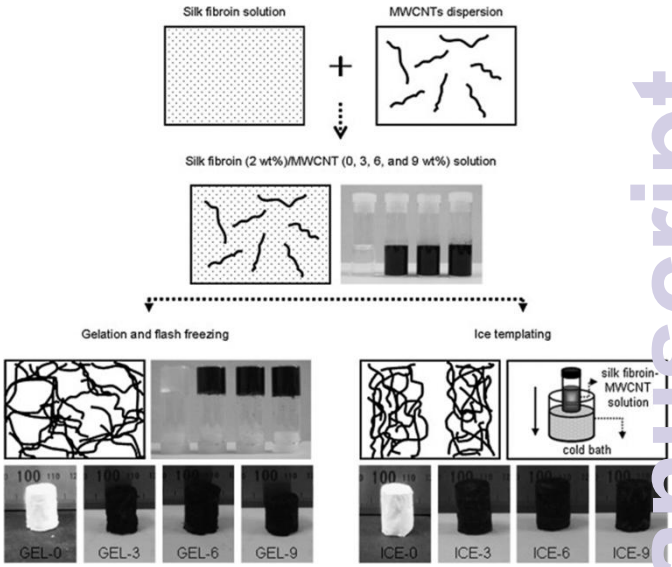

Figure 5. Schematic of fabrication procedure for the preparation of MWNTs aligned and non-aligned cryogels using silk fibroin as a crosslinker (Reproduced with permission.[60] Copyright 2009, Elsevier B.V.).

In addition to chitosan, other green dispersants and crosslinkers can also be used for the fabrication of CNTAs. Kwon and coworkers [60] used silk fibroin as a crosslinker to prepare MWNTs aligned and non-aligned cryogels through the procedure shown in **Figure 5**. In their procedure, MWNTs/silk fibroin suspension was cross-linked at 60 °C during a few days. Ice segregation method is used to form MWNTs aligned cryogels. Structure, morphology and functional properties of fabricated CNTs cryogels strongly depend on the preparation procedure and MWNTs concentrations.[60] DNA/protein-guided assembly can also be used for the preparation of SWNTs aerogel, as reported by Ostojic *et al.*[61] They prepared CNTAs through crosslinking of SWNTs/single-stranded DNA/streptavidin suspension. They claimed that four single stranded DNA in a DNA/streptavidin complex bind two SWNTs and as a result, a 3D SWNTs network cross-linked via DNA strands can be fabricated.[61]

A nondestructive method based on the assembly of CNTs 3D networks through π–π interaction of conjugated block copolymers and MWNTs surfaces is also reported by Zou and coworkers [62] as a promising method for the fabrication of CNTAs. A schematic of the gelation process of MWNTs aerogels using poly(3-hexylthiophene)-b-poly(3-(trimethoxysilyl) propyl methacrylate) (P3HT-b-PTMSPMA) as a crosslinker is illustrated in **Figure 6**. The lowest MWNTs critical gelation concentration (0.3 mg/mL) for the fabrication of CNTAs is reported when a conjugated block copolymer was used as the chemical crosslinker of MWNTs. The observed low critical gelation concentration is related to the presence of strong interactions between MWNTs, which originate from the chemical bonding of poly(3-(trimethoxysilyl) propyl methacrylate).[62]

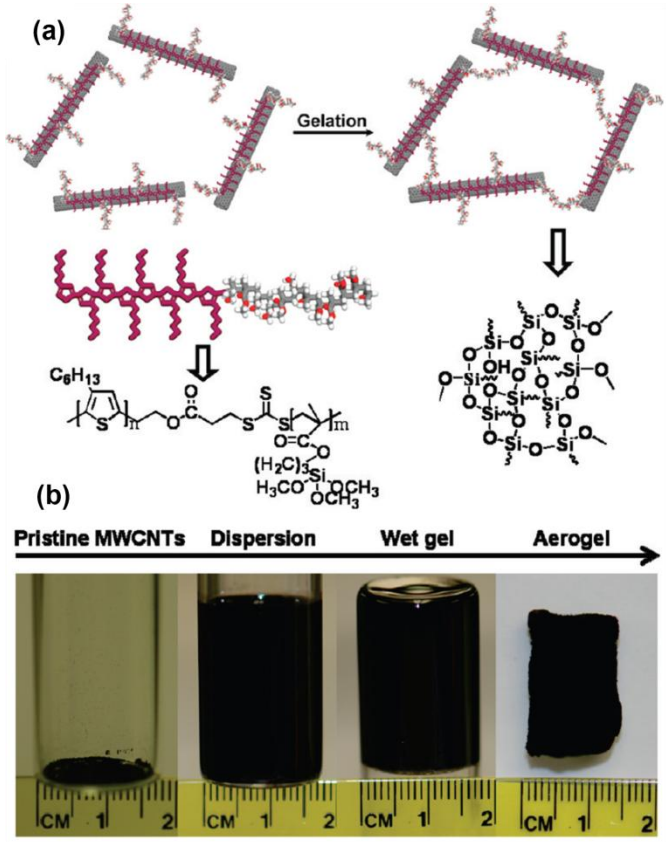

Figure 6. Schematic of gelation process of MWNTs using P3HT-b-PTMSPMA as a dispersant and crosslinker (a) and apparent conditions of dispersant and fabricated gels through preparation steps (b) (Reproduced with permission.[62] Copyright 2010, American Chemical Society).

In general, structural and physical properties of CNTAs strongly depend on the preparation mechanism as well as fabrication conditions. CNTs concentration through assembly system affects structural density and performance of final aerogel. Moreover, chemical binders can form more stable and consolidated aerogels. These crosslinking chemicals may ha a protein, polymeric or even green origins. A comparison between structural performances of self-assembled CNTA cross-linked using different chemical binders is presented in **Table 2**.

An almost same overall procedure is reported for the fabrication of self-assembled GAs.[8] The overall fabricatio process includes three individual steps: (i) preparation of a stable dispersion of functionalized graphene, (ii) assembly o graphene hydrogel from graphene suspension and (iii) conversion of prepared hydrogel into GA using a drying technique. In all cases, graphene oxide (GO) has been used as the starting point for the self-assembly process. GO can b readily dispersed in water and organic solvents to prepare stable suspension of dispersed GO.[63] The GO suspension ca form a 3D network through the hydrothermal reductio process.

Conditions of the reduction process as well as GO concentrations (C/O atomic ratio) dictate structure properties of GAs. Two kinds of structures are expected through hydrogen-bonding of GO nanosheets during reduction process, as reported by Wu *et al.*[64] Parallel G nanosheets form ordered structures and non-parallel nanosheets produce amorphous structures. Both structure form during a self-assembly process and final structure o aerogel depends on the ratio of these alternative structures. A schematic representation of two suggested self-assembl mechanisms as well as transmission electron microscopy (TEM) images of these structures are presented in **Figure 7**.

Table 2 Structural characteristics of CNTAs prepared using different gelation conditions and crosslinkers

CNTs type	CNTs content (wt. %)	Dispersant agent	Crosslinking agent	Gelation mechanism	Density (g/cm^3)	S_{BET} (m^2/g)	V_{micro} (cm^3/g)	V_{meso} (cm^3/g)	Reference
SWNTs	20-50	PPE	PPE	chemical cross-linking and CO2 supercritical drying	0.009-0.01	145-635	--	0.49-0.93	59
DWNTs	20-50	PPE	PPE	chemical cross-linking and CO2 supercritical drying	0.008-0.01	141-684	--	0.46-1.22	59
MWNTs	9	carboxylic functional groups	silk fibroin	gelation and flash freezing	--	115	0.0098	0.8609	60
MWNTs	9	carboxylic functional groups	silk fibroin	ice-templating	--	181	0.0251	0.6196	60
MWNTs	1	P3HT-b-PTMSPMA	PTMSPMA	gelation and freeze drying	0.004	580	--	--	62

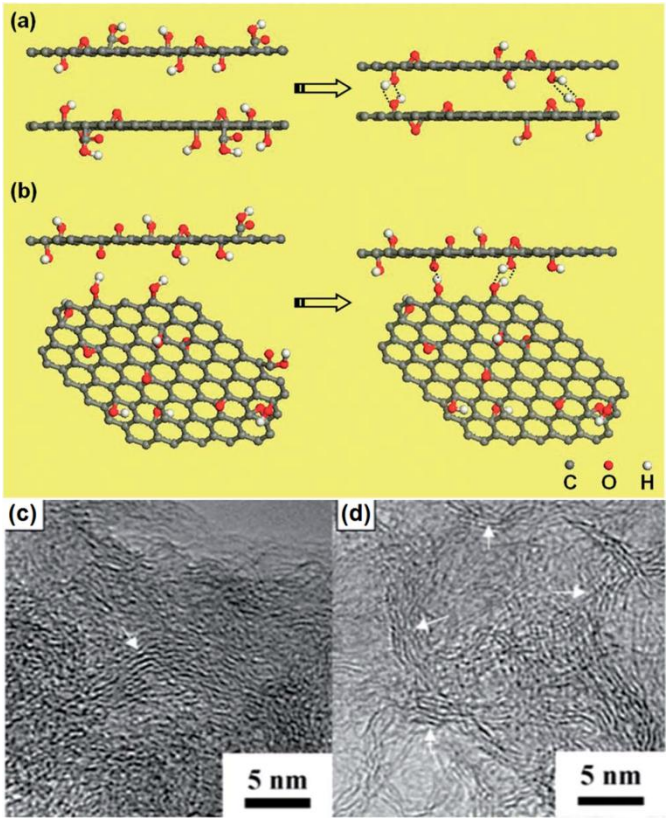

Figure 7. Schematic presentation of self-assembly mechanism of two parallel GO sheets (a), and two non-parallel sheets (b) as well as corresponding TEM images of GAs (c, d) (Reproduced with permission.[64] Copyright 2012, Royal Society of Chemistry).

Different reduction agents can be used as an aid to the self-assembly process. However, reduction process can be done without using any reducing agents. Xu and coworkers [9] reported preparation of graphene hydrogels through hydrothermal reduction of 1 and 2 mg/mL GO suspensions at 180 °C for 1-12 hours without using any reducing agents. They show that C/O atomic ratio as well as duration of hydrothermal process affect elasticity and conductivity of final products. In addition, GO suspension can be converted into graphene hydrogel through freezing using methanol and dry-ice.[65, 66]

L-ascorbic acid (LAA) is an environmental friendly widely used reducing agent with a promising reducing efficiency in the reduction of GO into graphene.[67] Unlike other reducing agents, such as sodium borohydride or hydrazine, no gas is formed as a by-product of the reduction reaction using LAA, which reduces the probability of inducing damages to the porous structure of GAs.[67, 68] Sui and coworkers [69] investigated the influences of different ratios of LAA to GO on the structure of final GAs. They suggested that LAA:GO ratio should be 1:1 higher to form a proper graphene hydrogel through reduction process at temperatures around 25-80 °C. Moreover, Fan *et al.*[70] investigated effects of variation in hydrothermal GO reduction conditions on the structural performance of GAs in the presence of LAA as the reducing agent. Results reveal that surface area and porosity of GAs are strongly depended on the GO concentration as well as reduction conditions.

As discussed, different reducing agents as well as crosslinkers can be used for the assembly of graphene hydrogels. Chen and coworkers [71] prepared GAs using various reducing agents such as $NaHSO_2$, Na_2S, Vitamin C, and hydroquinone. In addition, they show that shape of the 3D architectures can be controlled by changing the reactor type. Moreover, in another work they show that $NaHSO_3$ can be used as reducing agent as well.[72] Hypophosphorous acid and iodine (HPA-I) solution is also reported as a reducing agent for the hydrothermal reduction of GO suspension.[73] **Table 3** represents a comparison between structures of GAs reduced using different reducing agents.

One can also advance the structure of GAs using different crosslinkers to enhance interconnectivity by increasing the number of chemical and physical crosslinks. Bai and coworkers [74] reported that gelation of GO can be promoted by different non-covalent molecular interactions, including hydrogen bonding, π-stacking, electrostatic interaction, and coordination. Structures of several crosslinkers used to prepare graphene hydrogels are presented in **Figure 8**. They suggested that increasing the bonding force or decreasing the repulsion force between GO sheets result in GO gelation.

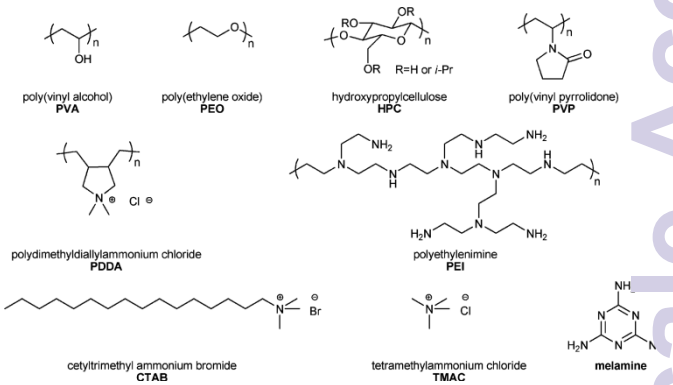

Figure 8. Chemical structure of crosslinkers used for the promotion of GA structure (Reproduced with permission.[74] Copyright 2011, American Chemical Society).

Table 3 Assembly conditions and structural characteristics of GAs

GO concentrations (mg/ml)	Reducing agent	Hydrothermal temperature (°C)	Hydrothermal duration (h)	BET Surface area (m^2/g)	Average pore size (nm)	Pore volume (cm^3/g)	Density (g/cm^3)	Reference
1	LAA	70	40	284	3.6	0.51	0.018	70
2	LAA	70	40	302	4.1	0.63	0.026	70
6	LAA	70	40	365	3.9	0.72	0.056	70
12	LAA	70	40	473	4	0.95	0.067	70
2	LAA	70	5	560	3.9	1.09	0.018	70
2	LAA	70	10	438	4	0.88	0.020	70
2	LAA	70	20	381	3.9	0.74	0.022	70
2	LAA	70	40	302	4.1	0.63	0.026	70
2	LAA	45	40	577	4	1.17	0.025	70
2	LAA	70	40	302	4.1	0.63	0.026	70
2	LAA	95	40	245	3.8	0.46	0.035	70
3	LAA	95	1.5	394	3.7	1.46	0.042	67
3	LAA	95	3	189	3.7	1.05	0.048	67
3	LAA	95	6	148	3.7	0.60	0.061	67
3	LAA	95	12	136	3.7	0.48	0.079	67
3	LAA	95	24	133	3.6	0.42	0.085	67
2	LAA	95	24	121	3.7	0.36	0.098	67
5	LAA	95	24	150	3.7	0.72	0.099	67
10	LAA	95	24	156	3.7	0.93	0.067	67
0.5	HPA-I	90	12	35	--	--	0.006	73
1	HPA-I	90	12	59	--	--	0.009	73
2	HPA-I	90	12	119	--	--	0.011	73
3	HPA-I	90	12	157	--	--	0.013	73
1.5	$NaHSO_3$	95	3	95	2-100	0.28	0.042	72
2	Gallic acid	95	8	299	--	--	0.013	75
2	Gentisic acid	95	8	109	--	--	0.014	75
2	Protocatechuic acid	95	8	140	--	--	0.016	75
2	Vanillic acid	95	8	184	--	--	0.012	75
2	Ferulic acid	95	8	347	--	--	0.017	75
5	--	85	72	867	8.6	1.90	--	64

Ji and coworkers [76] used glucose, *β*-cyclodextrin and chitosan as reducing agents in order to control and tailor the structure and morphology of GAs. Morphology of prepared GAs using each crosslinker is compared with the morphology of GA prepared without any crosslinker in **Figure 9**. They show that following same self-assembly procedure with glucose, *β*-cyclodextrin, and chitosan solutions, employing the same recipe of the graphene-based aerogels' gelation, but without GO, do not result in formation of hydrogels. This indicates that these carbohydrates (glucose, *β*-cyclodextrin, and chitosan) play a reducing agent role in the GO self-assembly process.

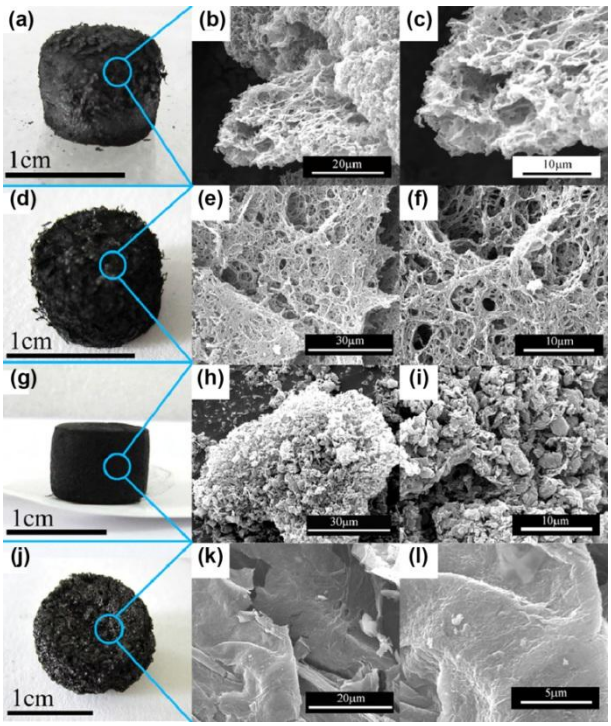

Figure 9. Optical images and SEM images of the GA sample (a, b and c) as well as self-assembled GAs prepared with the assistance of glucose (d, e and f), *β*-cyclodextrin (g, h and i), and chitosan (j, k and l) (Reproduced with permission.[76] Copyright 2013, Elsevier B.V.).

2.3. Nanocomposite carbon aerogels

Nanocomposite carbon aerogels can be classified into three categories: polymer/graphene aerogels (PGAs), polymer/CNTs aerogels (PCNTAs) and graphene/CNTs aerogels (GCNTAs). PGAs are mostly prepared through sol-gel polymerization of RF systems in the presence of GO in the sol phase.[77-81] In this process, a stable suspension of GO with a desired GO concentration can be mixed with specific resorcinol:formaldehyde and resorcinol:catalyst (sodium carbonate) ratios under sonication to form a so-gel mixture. The sol-gel mixture then should be placed in a mold and sealed to cure at a cure temperature around 85-90 °C.[79, 80, 82] Worsley and coworkers [79] reported that required time for cure process can vary between 12 to 72 h. The resulting gel can then be solvent exchanged with acetone and dried using supercritical CO_2. Prepared organic-based aerogel can be pyrolyzed then to form a PGA.

Lee *et al.* [83] reported a very same procedure for the fabrication of polyethyleneimine-modified PGAs. They have modified GO surface with polyethyleneimine (PEI) to prepare a modified-GO suspension, which then was used for the fabrication of PGAs. Preparation procedure used by Lee *et al.* for the fabrication of PGAs is depicted in **Figure 10**. PEI, however, can also directly be used as a crosslinker to form PEI-graphene aerogel, which can be pyrolyzed to form PGAs.[84] Other organic systems (such as phenol-formaldehyde and resol) and polymers (such as poly(amic acid), poly(dimethylsiloxane) and polystyrene sulfonate) can also be used as the crosslinker to form PGAs.[85-89]

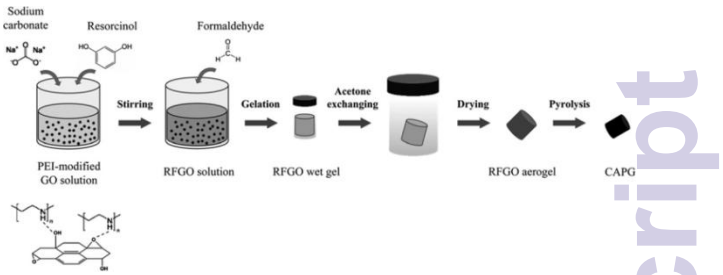

Figure 10. Preparation procedure for the fabrication of PGAs (Reproduced with permission.[83] Copyright 2013, Elsevier B.V.).

The sol-gel polymerization of RF system, described above, can also be used for the fabrication of PCNTAs.[90, 91] Presence of CNTs in the sol mixture during polymerization of RF system results in a CNTs 3D network cross-linked via polymer macromolecules. Prepared organic-based hydrogel can be dried and pyrolyzed to form PCNTAs. Moreover, Kim and coworkers [92] reported a method for the fabrication of poly(dimethylsiloxane) (PDMS)/SWNTs aerogels. In this method, vacuum suction was used to backfill CNTA with PDMS followed by curing PDMS at 70 °C. The resultant PDMS/SWNTs composite aerogel was highly bendable, deformable, and stretchable.

With using a mixture of GO and CNTs as the precursor of the self-assembly fabrication process, one can prepare GCNTAs through the hydrothermal process.[93] Hydrothermal reduction of GO and CNTs suspension can be done with and without using a reduction agent. Fan *et al.* [94] reported preparation of GCNTAs using LAA as the reduction agent for the hydrothermal reduction of GO/MWNTs stable suspension. Zhang and coworkers [95] reported a fabrication method for the preparation of GCNTAs using hydrothermal reduction of GO/CNTs suspension without using any reducing agent. They suggested three possible mechanisms for the hydrothermal reduction of GO/SWNT suspension, shown in **Figure 11**.

Zhang *et al.* [95] suggested three following mechanisms for the hydrothermal reduction of GO/SWNTs suspension: (i) recovery of π-π conjugations through elimination of OH and H groups at the edge of GO nanosheets during reduction process, (ii) crosslinking of hydroxyl and carboxylic groups, presence at the surface of GO and oxidized-SWNTs, and (iii) formation of 3D network through vacancies and topological defects, formed through release of carbon dioxide during thermal treatment. Zhang and coworkers suggested also that these mechanisms could occur in parallel during the hydrothermal reduction process of GO/SWNTs system.

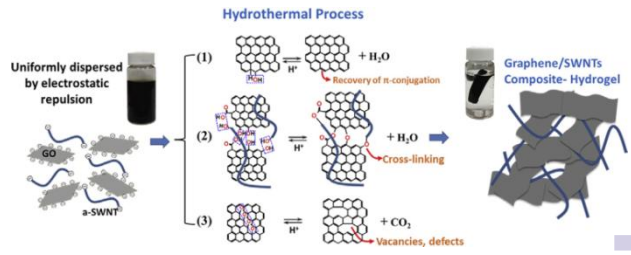

Figure 11. Suggested mechanisms for the hydrothermal reduction of GO/SWNT system (Reproduced with permission.[95] Copyright 2013, Elsevier B.V.).

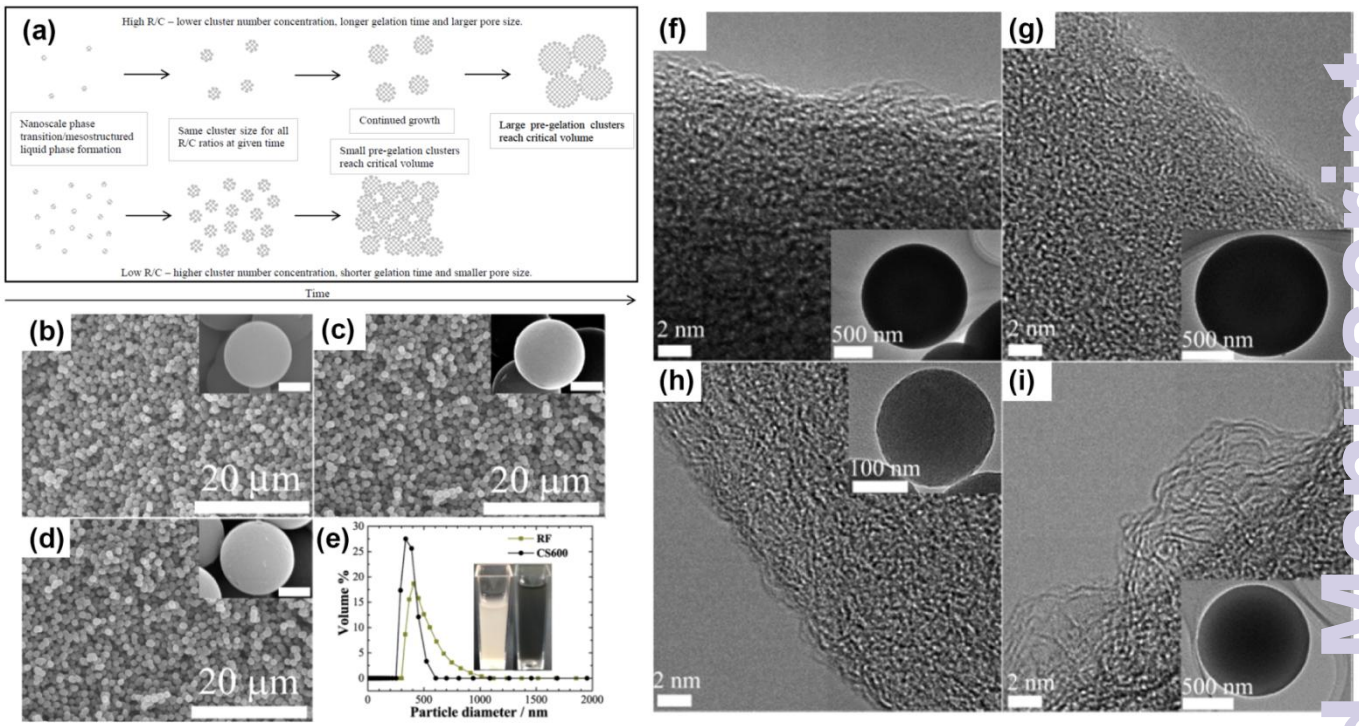

Figure 12. Schematic representation of cluster formation and growth process in sol-gel polymerization of RF system (a) (Reproduced with permission.[96] Copyright 2014, American Chemical Society), SEM images of typical: RF aerogel spheres (b), CA spheres pyrolyzed at 600°C (c), CA spheres pyrolyzed at 900°C (d), DLS plots of separate batch of RF aerogel and CA spheres (e), HR-TEM images of typical: RF aerogel spheres (f) CA spheres pyrolyzed at 600°C (g), CA spheres pyrolyzed at 900°C (h) and CA spheres pyrolyzed at 1100°C (i) (Reproduced with permission.[97] Copyright 2014, American Chemical Society).

3. Structural characteristics of carbon aerogels

Structural performance of a carbon aerogel is strongly depended on fabrication conditions as well as nature of precursor. The gelation process of carbon aerogels, prepared through well-known sol-gel method, initiates with formation of primary nanoparticles from sol suspension. Primary nanoparticles, then, aggregate to form clusters which in turns, crosslink to form secondary nanoparticles.[98] Secondary nanoparticles in the structure of conventional pyrolyzed carbon aerogels are expected to have a semi-spherical geometry.[96, 99, 100] Spherical geometries of secondary nanoparticles in the structure of carbon aerogels prepared through pyrolysis of a set of controlled RF systems are depicted in **Figure 12**.

In conventional aerogels, however, an inter-particle neck presence between two adjacent secondary nanoparticles, which controls structural and physical performance of aerogel. Thermal conductivity, electrical resistivity and mechanical strength of aerogels are directly influenced by this neck region.[97, 101] Interconnectivity of secondary nanoparticles is directly affected by density of aerogel. The higher concentration of polymer chains in the structure of aerogel results in higher connectivity of spheres and smaller porous volumes.[101] **Figure 13** shows the dependency of secondary nanoparticles geometrical state on the density of aerogel for a polyurea aerogel (PUA) fabricated through sol-gel polymerization.

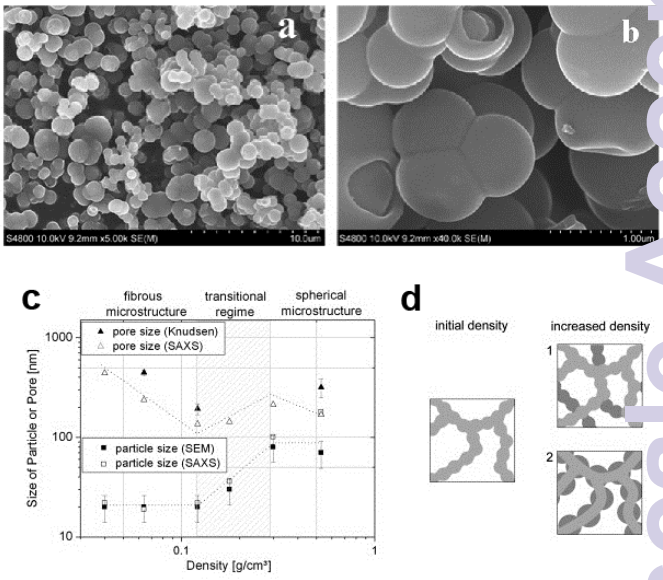

Figure 13. SEM images of CAs spheres interconnected through neck area (a and b) (Reproduced with permission.[97] Copyright 2014, American Chemical Society), dependency of particle and pore size on aerogel density for a PUA (c) and schematic representation of interconnectivity variations between secondary nanoparticles with an increase in density (d) (Reproduced with permission.[101] Copyright 2013, Elsevier B.V.).

Size of spherical nanoparticles is also a structural characteristic of CAs, which strongly depends on the fabrication process. Presence of surfactants in the sol suspension, through sol-gel

process, is reported to result in formation of more spherical-like nanoparticles. Moreover, Wu and coworkers [102] reported that higher surfactant concentrations led to the smaller particle sizes and the greater dispersed intermediate numbers. However, Tonanon *et al.* [103] found that one can fabricate CAs with different morphologies and porous properties using different types of surfactants. SEM images of CAs prepared through sol–gel polycondensation of RF system followed by inverse emulsion polymerization, freeze drying and pyrolysis, in the presence of different types and concentrations of surfactants, are shown in **Figure 14**.

A typical XRD pattern of CAs and a comparative graph of XRD patterns of graphite, activated carbon and CAs, prepared through pyrolysis of RF precursor, are shown in **Figure 15**. Normally, XRD pattern of CAs contain two peaks at 2θ values around 23.5° and 43.5° which originate from strong (0 0 2) and weak (1 0 1) carbon diffractions, respectively.[12, 104, 105] As argued by Lin and Ritter, by comparing XRD patterns of CAs, graphite and activated carbon, it can be concluded that CAs are not completely amorphous.[106] Conventional CAs are considered as partly graphitized carbon materials with some graphite-like carbon structures interconnected via amorphous carbons.[104]

Gelation process of RF system results in formation of a crosslinked elastic gel with a porous microstructure. One can determine gelation time for RF systems, which is defined as the time that grown clusters interconnect to form a monolith gel, from the intersection of the storage (G') and loss (G") moduli versus time curves. Job and coworkers [107] argued that the gelation time is highly affected by reaction temperature and R/C ratio. They believed that gelation time in a RF system decreases with temperature increasing and R/C ratio decreasing.[107] Regarding elastic performance of RF systems, Gross *et al.* [108] shown that drying process has a high influence on elastic behavior of RF gels. Moreover, they have shown that solvent exchange process does not significantly affect the elastic behavior of RF gels.[108]

Porosity is the other important microstructural characteris of CAs which strongly depends on synthesis conditions, solven exchange, drying, and carbonization process.[109-111] Schaefe and coworkers [112] suggested that porous structure of RF gels originates from nanoscale phase separation in the solutio precursor, which induced and limited by crosslinking process. They suggested that branched polymer system become incompatible with the solvent through crosslinking. This incompatibility results in nanoscale phase separation, which i turns leads to the formation of porous structure of RF gels.[11] Regarding influences of sol-gel conditions on porosity, detailed studies by Mirzaeian and Hall revealed that R/C ratio dictated total pore volume of RF gels.[111] The noticeable influence of R/ ratio on porosity of RF systems is related to the effects tha this ratio has on inter-particle crosslink density.

Resorcinol anions form through reaction of resorcinol an formaldehyde in the presence of catalysts, which are m reactive than uncharged resorcinol molecules. Therefore crosslinking process increases in the case of more R/C ra and as a result, mesoporosity of the RF gel increase. Mirzaeian and Hall suggest that high catalyst contents in the sol g process results in formation of small secondary nanoparticles which in turns leads to the formation of microporous structures. On the other hand, low catalyst contents throug polymerization process results in formation of large nanoparticles and development of mesoporosity.[111] Feng *et al.* [113], however, suggest that R/C ratio should not be less tha 300 to prevent structural shrinkage induces by low nanoparticle size and pore volume. Moreover, they sugges that higher W/R ratio results in lower density and larger pores in the structure of RF gel and as a result, less shrinkage durin carbonization of RF system.[113]

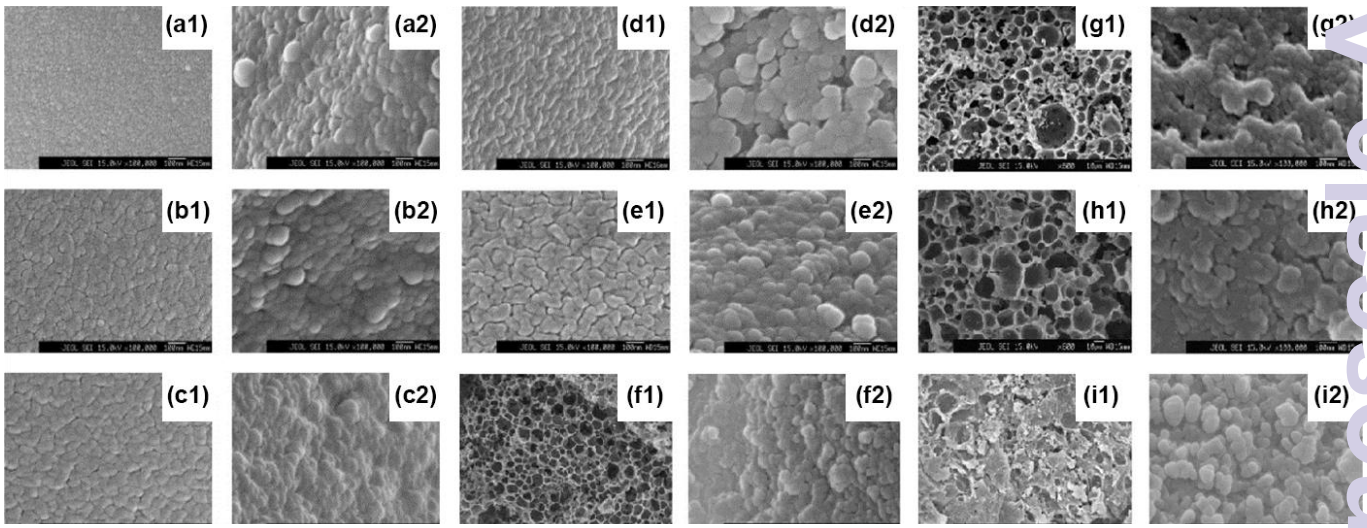

Figure 14. SEM images of carbon cryogels prepared through polymerization of RF system (R/C=400; R/W=0.25; T_{gel}=298 K; T_{pyro}=1023 K) in the presence of 10.0 (a), 5.0 (b), 2.5 (c), 1.0 (d) and 0.5 vol.% (e) SPAN80 (nonionic surfactant) as well as FC4430 (nonionic fluorinated surfactant); R/C=100; C/W=45; R/W=0.50; vol.%=3.80 (f) an vol.%=0.84 (g), R/C=400; C/W=6; R/W=0.25; vol.%=0.84 (h) and vol.%=3.80 (i) (Reproduced with permission.[103] Copyright 2003, Elsevier B.V.).

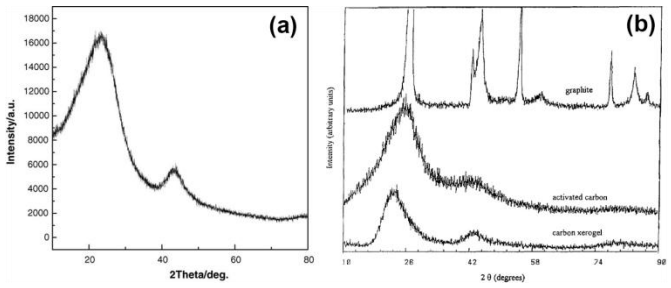

Figure 15. XRD pattern of a typical CA prepared through pyrolysis of RF system at 800°C (a) (Reproduced with permission.[104] Copyright 2006, Elsevier B.V.) and a comparative XRD graph of a typical carbon xerogels, activated carbon and graphite powder (b) (Reproduced with permission.[106] Copyright 1997, Elsevier B.V.).

The microporosity of RF gels does not depend on the nature of solvent used for the solvent exchange process.[114] Moreover, drying process does not affect microporosity of organic gels.[110] Mesoporosity, however, is reported to be affected by applied drying method.[110] Compared to supercritical drying, freeze-drying is reported to result in formation of larger mesopores in RF aerogels.[115] As discussed before, the main reason for the formation of such a mesoporous structure is ice crystal growth, which takes place during the freeze-drying process.[116] Moreover, carbonization process is reported to impact microstructure of CAs, as some micropores take place during pyrolysis of RF systems.[111] Generally, it has been suggested that carbonization of RF systems results in more meso- and microporosity and larger surface area.[111]

Formation steps, morphology and structural properties of self-assembled GAs, prepared through reduction process in the presence of sodium ascorbate as reducing agent at 90°C, are presented in **Figure 16**. Based on the used reducing agent, phase separation in the gelation process of GO suspension to GAs can last from one to several hours.[117-119] However, further hydrothermal reduction results in more reduction of GO nanosheets and more π-π conjugation between graphene structures.[118] Moreover, long hydrothermal reaction leads to an increase of the intensity ratio of D/G bands in Raman spectroscopy results, which indicates the formation of more reduced graphene nanosheets.[119] Same structural performance is reported by Ostojic for self-assembled CNTAs.[61] The presence of D band in Raman spectra of CNTAs, which is associated with *K* point vibrations, implies a non-covalent gelation process.[61]

SEM observations reveal that GA structure becomes more tightly assembled with reduction progressing.[117] Therefore, it can be concluded that gelation process of GAs is based on the reduction of GO nanosheets through the hydrothermal process. In addition, π-π interactions between graphene nanosheets, which are responsible for non-covalent crosslinks in the structure of GAs, increase with hydrothermal reaction time. Rheological behavior of GO suspension through the gelation process shows an almost frequency-independent behavior for storage modulus (G') and an elastic-gel behavior for loss modulus (G").[117] Moreover, formation of π-π interactions between reduced graphene nanosheets through the reduction process is obvious in UV-Vis and XPS results. XRD pattern of GAs contain a broad peak at 2θ values around 25°. This peak is reported as the significant peak of π-π conjugated graphene nanosheets in the structure of GAs.[64, 70, 117, 119]

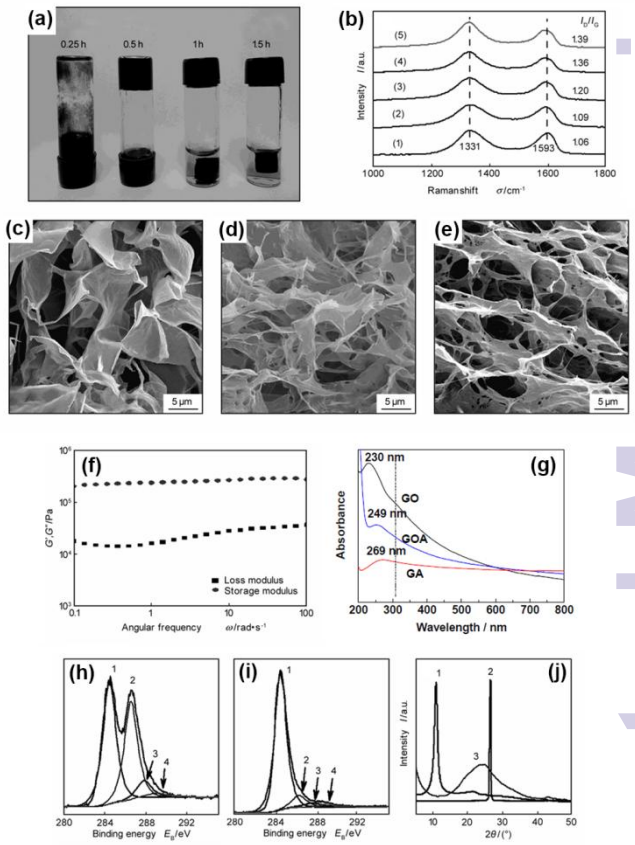

Figure 16. Images of assembly glass vial through gelation process (a), Raman spectra of GO gels after (1) 0, (2) 0.25, (3) 0.5, (4) 1.0, (5) 1.5 h reduction (b), SEM images of GO gels after 0.25 h (c), 0.5 h (d) and 1 h (e) of hydrothermal reduction, rheological behavior of GA through gelation process (f) (Reproduced with permission.[117] Copyright 2011, Elsevier B.V.), UV-Vis spectra of GO and GA (g) (Reproduced with permission.[64] Copyright 2012, The Royal Society of Chemistry), XPS spectra of GO and GA (h, i) and XRD patterns of GO (1), natural graphite (2) and freeze-dried GA (3) after gelation (j) (Reproduced with permission.[117] Copyright 2011, Elsevier B.V.).

In the case of PGAs, structural performance of aerogel is also depended on polymer matrix, besides GO nanosheets. Structural characteristics and morphological properties of PGAs as a function of GO loading contents are presented in **Figure 17**. XRD pattern of GO loaded phenol/formaldehyde (PF) xerogels, as expected, contains only the broad characteristic peak of GAs and there is no sign of characteristic peak of GO nanosheets, nor peaks of the PF system. Through carbonization process, however, a peak at 44° appeared which is due to the growth of crystalline structures in the PF secondary nanoparticles through pyrolysis. Same behavior is reported for the different loading contents of GO nanosheets in RF systems.[77, 80]

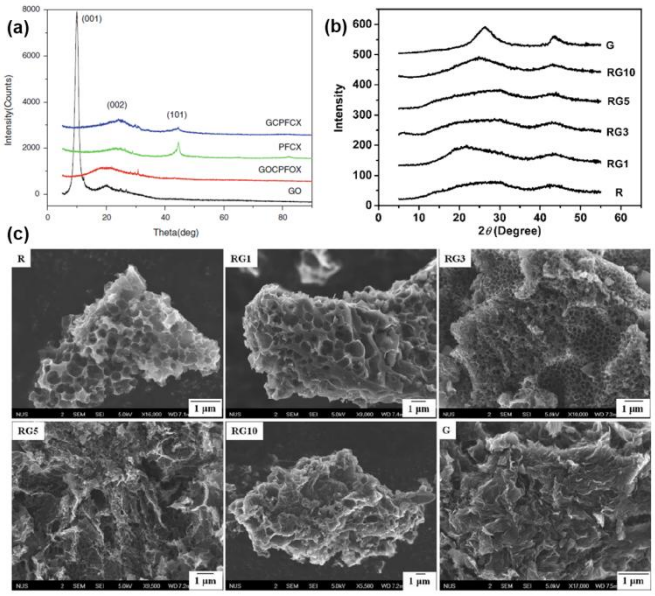

Figure 17. XRD patterns of GO nanosheets, GO loaded PF xerogel (GOCPFOX), carbonized PF xerogel (PFCX) and carbonized GO loaded PF xerogel (GCPFCX) (a) (Reproduced with permission.[85] Copyright 2013, Springer Science+Business Media), XRD patterns (b) and SEM images (c) of activated carbonized RF gel (R), 1, 3, 5, and 10 weight % GO loaded carbonized RF aerogels (RG) and GA (G) (Reproduced with permission.[80] Copyright 2011, The Royal Society of Chemistry).

Worsley and coworkers [77] reported that morphology of PGAs, prepared through carbonization of GO and RF systems, is strongly depended on the contents of RF system in PGA. Higher GO to RF contents, results in formation of PGA with no sign of individual RF secondary nanoparticles. A higher content of RF, however, leads to formation of PGA structures with distinguishable secondary nanoparticles. It is helpful to note here that the morphology of activated carbon structures of RF system also changes in the presence of GO nanosheets to sponge-like structure bearing cavities with small pores.[80]

XRD pattern of GCNTAs contain a broad peak at 2θ values around 25°, similar to the XRD pattern of GAs.[93-95, 120] This broad peak is related to the non-crystalline π-π stacked graphene nanosheets in the structure of GCNTAs.[94] Such a structural performance is in consistence with morphology of GCNTAs, which is a macro-porous network with graphene nanosheets walls. Shao *et al.* [120] suggested that a sandwich morphology form during the hydrothermal process of GO nanosheets with SWNTs stacked between GO nanosheets. Moreover, the ratio of D/G Raman peaks of GCNTAs increases with the content of SWNTs. This behavior is related to the increment of perfect graphitic structures with the increase in the content of SWNTs in the structure of GCNTAs. Structural characteristics and morphology of GCNTAs are shown in **Figure 18**.

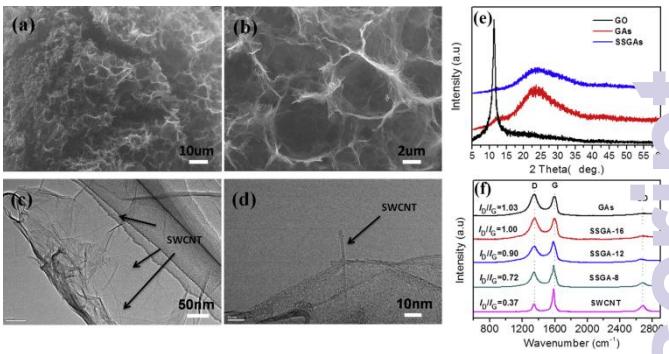

Figure 18. SEM (a, b) and TEM (c, d) images of GCNTAs, XRD patterns (e) and Raman spectroscopy (f) results of GO nanosheets, GAs and GCNTAs fabricated through hydrothermal reduction of GO-SWNTs suspension with 8, 12 and 1 weight % SWNTs (Reproduced with permission.[120] Copyright 2014, Elsevier B.V.)

4. Properties and applications

During recent years, carbon aerogels have attracted a gr[eat] interest for many industrial and special applications. High specific surface area, great porosity, enormous electrical conductivity and low density of these materials made them promising candidates for many novel and comm[on] applications in different industries. Moreover, high oil uptak[e] of novel GAs and CNTAs, as well as conventional CAs ha[ve] lightened an important way for environmental applications o[f] these materials.[121-123] Plenty of important applications can b[e] named for carbon aerogels such as water purification [124] catalysts [4], supercapacitors [87] and thermal insulatin[g] materials.[125] Electrical performance and thermal characteristics of carbon aerogels, which made them a perfe[ct] candidate for the latter two application fields, are discussed throughout this section in details.

4.1. Electrochemical properties and applications

From the very beginning, considerable efforts were devote[d] on developing novel potential applications for carbon aeroge[ls]. One of the most interested applications of carbon aerogels is in the fabrication of highly efficient electrodes, considering noticeable electrochemical and electroanalytical properties o[f] these materials.[126] Energy is stored in supercapacitors through separation of charge across the electrode/electrolyte interface. Therefore, there are four requirements for [a] material to be a good electrode: (1) high surface area, (2) high electrical conductivity, (3) high polarizability, and (4) n[o] participation in faradaic reactions.[127]

High current-density, controllable pore size, low electric[al] resistance, low detection limits and low dependency on convective transport are some advantages of CAs, whic[h] consist of the conductor ordered regions separated by disordered insulator parts.[127, 128] High specific surface are[a] (about 750 m^2/g; see Table 1) of CAs results in lots of available active sites, which facilitate reversible intercalation of lithium ions. Activation of CAs by CO_2 is reported as a promising method for increasing available surface area of CAs. Optimum activation parameters, however, should [be]

considered to achieve maximum specific surface area from RF system.[26] Moreover, initial pH of RF solution, carbonization temperature and R/C ratio, are three more parameters, which affect specific surface area of CAs.[130, 131]

Electrical conductivity of carbon aerogels highly depends on density of pyrolyzed aerogel. Carbon aerogels, prepared through carbonization of RF systems, are reported to have a wide range of electrical conductivity from 5 S/cm for a CA with a density of about 300 kg/m^3 to 20 S/cm for aerogel with a density around 600 kg/m^3.[132] In addition, a close accordance between elastic performance and electrical conductivity of these materials is reported by Saliger *et al.*[132] Generally, when features of high electronic conductivity, rapid ion transport and available active sites, all integrate in a material, it can be considered as a perfect candidate for the fabrication of supercapacitor electrodes. Hao *et al.* [133], hence, tried to present a correlation between electrochemical and structural features of CAs. Reported Correlations between capacity and crystalline parameters as well as textural parameters are presented in **Figure 19**. Results revealed that important electrochemical features of CAs strongly depend on the contents of crystalline and porous structures.[133]

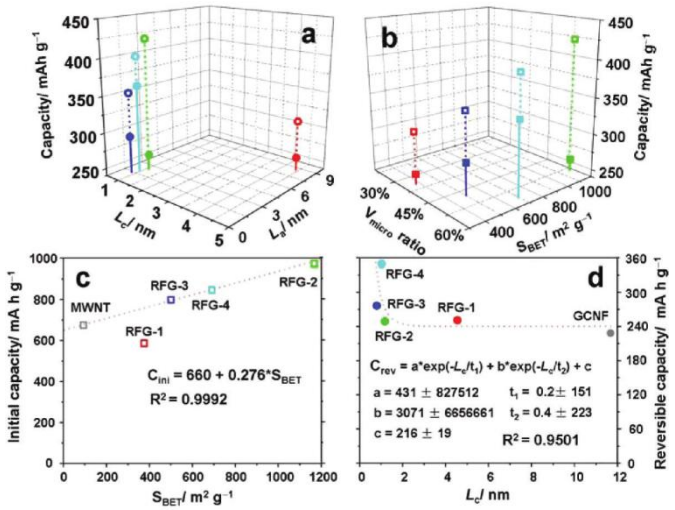

Figure 19. Correlation between the capacity and crystalline parameters (the average crystallite size in the a-axis direction: L_a and c-axis: L_c) (a), correlation between the capacity and textural parameters (V_{micro}/V_{total} ratio and S_{BET}) (b), the relationship between S_{BET} and the initial discharging capacity (c), and the relationship between L_c and reversible capacity after 50 cycles (graphitized carbon nanofibers: GCNF, RF gel pyrolyzed at 800°C for 2 hours: RFG-1, RF gel pyrolyzed at 850°C for 30 minutes: RFG-2, RF gel pyrolyzed at 800°C for 2 hours after treatment with acid: RFG-3, and RF gel pyrolyzed at 800°C for 2 hours with more porosity: RFG-4) (Reproduced with permission.[133] Copyright 2012, American Chemical Society).

Based on comparisons in Figure 19, presence of both graphitic and amorphous structures, moderate accessible surface areas, and highly interconnected pore channels result in high rate-performance, cycle stability, and lithium-ion storage capacity. In the case of initial efficiency, CA with the highest numbers of crystalline structures (RFG-1) presented the highest efficiency. Moreover, CA with the highest porosity (RFG-2) offered the highest initial charge/discharge capacity, but also the lowest reversible capacities. Furthermore, CA with moderate crystallinity (RFG-4) had the best reversible capacity and rate performance. Hao and coworkers [133], therefore, suggest that a correlation presence between structural characteristic of CAs and electrochemical performance of these materials.

Self-assembled GAs are also reported to have a high-rate supercapacitive performance with specific capacitance value around 211.8 and 278.6 F/g in KOH and H_2SO_4 electrolytes, respectively.[134] The extent of reduction is reported t significantly affect the electrochemical performance of GAs.[13] In addition, Chen and coworkers [135] reported that macropore and surface roughness were two other important factors in the structure of GAs, which affect electrochemical features through enhancement of hydrophilicity/hydrophobicity performance. Electrical conductivity of GAs is reported to var with the concentration of GO nanosheets in the initial G suspension. Electrical conductivity of GAs differs from 1.5 × 10 ^{2} S/m for the GA assembled from 1 mg/ml GO concentration to 1 S/m for a GA fabricated from20 mg/ml GO concentrat in the initial suspension.[136]

In comparison with CAs, PGAs are reported to have lar specific capacitance values (205 F/g), especially at high scan rates.[83] This increase in capacitance of these aerogels is rela to the higher specific surface area of PGAs, compared to CA prepared from RF system. Reported specific capacitance for PGAs, however, is still lower than the capacitance of GA However, GCNTAs are reported to have a 37% larger specif capacitance (245.5 F/g) in comparison with GAs. This significant increase in capacitance performance of composit aerogels is accompanied by a current density of 2.5 A/g in an aqueous electrolyte.[120] Moreover, a high energy-density o 80.0 Wh/kg is reported for GCNTAs in an ionic liquid electrolyte.[120]

4.2. Thermal insulating properties and applications

Low thermal conductivity of CAs was subjected to a great interest from the very beginning discovery of these mater s by Pekala.[2] Porous structure of CAs as well as high IR-extinction coefficient of these materials lead to low thermal conductivity values even at elevated temperatures.[137] Mor recent studies by Wiener and coworkers [138, 139] revealed that CAs are capable of preserving their porous structure even at ultra-high temperatures. Based on Wiener *et al.* [138, 139], th total thermal conductivity of CAs prepared from pyrolysis of R at 1800 °C is expected to be in the range of 0.05-0.5 W/m These results are in close accordance with the results reported by Feng et al. [140], which shown that the thermal conductivity o CAs at 1800 °C should be as low as 0.5 W/mK. Therefore, CAs can be considered as perfect candidates for high-temperature thermal insulating applications.

As noted before, low thermal conductivity of CAs is related t the porous structure of these materials. Presence of a stati gas (mostly air) in the porosity of CAs results in very lo gaseous thermal conductivity values. Moreover, high IR extinction coefficient of these materials (more than 10 m^2/kg) leads to very low radiative thermal conductivity value

even at elevated temperatures.[138] These low contributions of gaseous and radiative thermal conductivities into the total thermal conductivity of CAs made these materials comparable with SiO_2 and polymer aerogels for thermal insulating applications.[141] Contributions of radiative and gaseous thermal conductivity as well as total thermal conductivity of CAs at elevated temperatures are shown in **Figure 20**.

Just like other aerogel systems, total thermal conductivity of CAs is closely related to the density of aerogel. As reported by Feng and coworkers [142], however, this dependency increase with service temperature. Moreover, it is more likely that the dependency of CAs thermal conductivity is more related to the solid contribution than gaseous and radiative ones.[139] Reported results[138-140], however, prove that the total thermal conductivity of CAs is in a low range even at high temperatures and hence, these materials have a high potential for high-temperatures insulating applications.

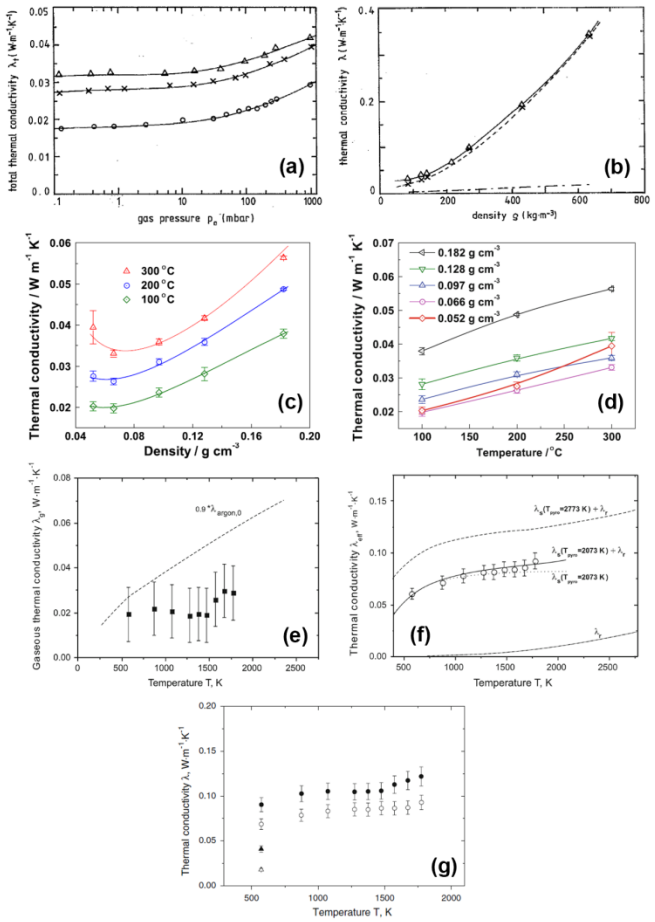

Figure 20. Thermal conductivity of CAs as a function of: air pressure at room temperature (○ : 82 kg/m^3; × : 124 kg/m^3; Δ : 139 kg/m^3) (a), aerogel density (Δ : in air and × : under pressure) (b) (Reproduced with permission.[137] Copyright 1993, AIP Publishing LLC), their densities under various temperatures in air (c), measuring temperature in air (d) (Reproduced with permission.[142] Copyright 2011, Springer Science+Business Media, LLC) as well as gaseous (e), solid and radiative (f), as well as total thermal conductivities (g) of CAs as a function of sample temperature (Reproduced with permission.[138] Copyright 2009, Springer Science+Business Media, LLC).

GAs, also, can be classified into thermal insulating materials category, as the total thermal conductivity of these aerogels differs from 0.04 to 0.36 W/mK.[136, 143] Based on reports by Tang *et al*. [136] and Fan *et al*. [143], thermal conductivity of GAs is strongly influenced by GO concentration in the initial suspension used for the fabrication of aerogel and as a result the density of aerogel. This behavior is similar to the one observed for CAs. Moreover, Fan and coworkers [143] revealed that heat treatment of GAs leads to a variation in thermal conductivity of aerogels. An increase in the thermal conductivity is reported in the case of GAs prepared from low contents of GO nanosheets in the initial fabrication suspension. Contrarily, thermal annealing of GAs prepared from GO suspension with high amounts of GO, resulted in a decrease in thermal conductivity of GAs.

They suggested that the observed increase in the case of GAs prepared from low GO amounts is related to the elimination of functional groups during annealing process.[143] Moreover, they believed that the observed decrease in thermal conductivity of GAs prepared from concentrated GO suspension is due to formation of graphite-like aggregated nanosheets through the heat treatment process.[143] Consequently, GAs can be considered as ultra-light insulating materials with low thermal conductivity.

4.3. Other application fields

In addition to thermal and electrochemical applications, plenty of application fields for carbon aerogels, in activated, hybrid, nanocomposite or doped forms, have been reported in the literature. Therefore, in addition to two discussed potential applications for pure carbon aerogels, which have been discussed in details through two preceding sections, some other application fields for carbon aerogels are reviewed in this section briefly.

One of the most interested applications for carbon aerogels and their derivatives is catalyst systems. The catalytic activity of catalysts in a medium depends on several factors, including contact area between the catalyst and the medium.[144] Only catalyst molecules which are in contact with medium are active and therefore, this feature is an important factor in selecting the appropriate catalyst support system. Nitrogen- and metal-doped CAs, GAs and CNTAs have been reported as promising candidates for such an application. Regarding metal-doped CAs, there are three main fabrication strategies: (i) addition of metal precursor to the initial organic sol mixture, (ii) ion-exchange of metal ions and polymer aerogel prepared from resorcinol-derivatives containing an ion-exchange moiety, and (iii) deposition of metal precursor on the organic or carbon aerogel (using impregnation or adsorption).[4]

Ábrahám and coworkers [145] used the third strategy to fabricate a CA-supported molybdenum catalyst for the hydroconversion reaction of acetic acid. They first prepared a CA through conventional pyrolysis of resorcinol-formaldehyde polymer aerogel, and then used the impregnation method to dope different molybdenum species in CA structure through a heat treatment process. Based on their report, the fabricated CA

supported molybdenum catalyst was catalytically effective in the hydrogenation reaction of acetic acid. Moreover, they suggested that accessibility of the carbon surface to the molybdenum sites as well as the amount and form of doped molybdenum molecules govern all three paths for the reduction of acetic acid (hydrogenolysis, ketonization, and consecutive reduction pathways). This is in close accordance with Smirnova *et al.* [144] report, which argued that pore size of aerogel supports has a huge influence on catalytic performance of metal-doped CA systems.

Carbon aerogels prepared from other precursor systems can also be used for the fabrication of catalyst systems. Guilminot and coworkers [146] used a cellulose-based carbon aerogel as platinum catalyst support. An organic aerogel was first prepared from crosslinking of cellulose acetate with polyfunctional isocyanate and by employing supercritical drying method. The prepared aerogel was then pyrolyzed under flowing nitrogen and activated in CO_2 atmosphere. The activation process was followed by an impregnation step to deposit platinum on the structure of activated aerogel. They suggested that pyrolysis temperature could have a great impact on the catalytic performance of metal-doped CAs, as the content of unstable groups in the structure of cellulose-based organic aerogels, which in turns dictates the number of available sites in the structure of final platinum-doped CA, can be controlled by the pyrolysis temperature.[146]

Du *et al.* [147] prepared a nitrogen-doped CNTA with a high catalytic performance for oxygen reduction reaction (ORR). A MWNTs suspension was first crosslinked through a hydrothermal reaction using pyrrole as the crosslinking agent. The fabricated gel was then pyrolyzed in the presence of pyrrole molecules as "built-in" nitrogen sources. This process resulted in the fabrication of a nitrogen-doped CNTA with a high conductivity (up to 10.9 S/m) and specific surface area (up to 869 m^2/g).[147] Prepared nitrogen-doped CNTA presented a remarkable activity toward ORR catalysis in alkaline environment. Moreover, Li and coworkers [148] prepared a recyclable CNTA-supported cadmium sulfide (CdS) as a photocatalyst hybrid system. Fabricated hybrid system had an improved catalytic efficiency, compared to TiO_2 nanoparticles. In addition, it was suggested that CdS nanoparticles grafted on the outside surface of CNTA were active sites in photocatalysis, while other CdS nanoparticles, anchored inside the CNTA, were fresh for use when the catalyst was recycled.[148]

As reported by Yin *et al.* [149], nitrogen-doped GAs can also be used for the ORR. They fabricated an iron nitride/nitrogen doped-graphene aerogel hybrid catalyst system through a two-step hydrothermal process, including a hydrothermal assembly process followed by an annealing step. Reported results demonstrated that surface area, porosity, density of Fe–N–C active sites, and size of particles on graphene can highly affect the ORR catalytic performance of the system. Wu and coworkers [150] also reported fabrication of a nitrogen-doped GA-supported metal-oxide (Fe_3O_4) catalyst system for the ORR. Their results revealed the importance of 3D macropores and high specific surface area of the GA support, as more positive onset potential, higher cathodic density, lower H_2O_2 yield, and higher electron transfer number for the ORR were achieved when nitrogen-doped GA was used instead of nitrogen-doped carbon black or nitrogen-doped graphene sheets as Fe_3O_4 nanoparticles support system.

GAs can also be used in the fabrication of high-performance lithium-ion batteries (LIBs). Jiang and coworkers [151] reported the use of a SnS_2/GA system, with high reversible capacity (655 mA.h/g after 30 cycles) and excellent rate capability (240 mA.h/g at the rate of 1000 mA/g), as an anode in rechargeable LIBs. Such a performance was related to the high surface area, 3D macroporosity and high electrical conductivity of fabricated 3D structure, as well as improved contact area (and synergistic interactions as a result) between SnS_2 and the graphene. Qiu et al. [152] prepared a TiO_2/GA system with a high-potential applicability as both air purification and LIBs. They used glucose as the crosslinking agent for the hydrothermal assembly of GA in the presence of TiO_2 nanocrystals. Besides enhanced photocatalytic performance, the fabricated system presented excellent specific capacity, high lithium storage, highly reversible capacity, and excellent rate performance.

Carbon aerogels can also be used for the fabrication of novel polymeric nanocomposite systems. Huang and coworkers [153] used GAs for the preparation of an inorganic–organic double network hydrogel. They first prepared a graphene hydrogel from hydrothermal reduction of GO nanosheets, and then immersed hydrogel in acrylic acid monomer and polymerized monomers to form a graphene and poly(acrylic acid) nanocomposite aerogel system. The prepared nanocomposite system performed interesting flexibility and electrical conductivity.[153] In addition to discussed potential application fields, carbon aerogels can be considered as candidates for hydrogen storage [154], fire-resistant systems [118, 155], heavy metal ions removal systems [123] and oil absorption [118, 1] applications.

5. Conclusions

In this review, synthesis procedure and mechanisms for the fabrication of different types of carbon aerogels, i.e. CAs, GAs, CNTAs, PGAs, PCNTAs and GCNTAs, were discussed and influences of variations in the synthesis conditions on the structure of carbon aerogels were covered. Conventional carbon aerogels are products of the pyrolysis process of organic aerogels and structure of these materials is strongly affected by synthesis conditions. The structure of these materials is also highly depended on the drying process as well as carbonization temperature.

The structures of GAs and CNTAs, on the other hand, is influenced by the concentration of GO and CNTs in the precursor suspensions, respectively. Structural characteristics of these materials are also dictated by the hydrothermal reduction process. PGAs and PCNTAs are products of sol-gel polymerization of an organic system in the presence of graphene (or GO) nanosheets and CNTs in the sol suspension, respectively. The structural performance of these materials is also highly affected by the conditions of the polymerization process, as well as GO and CNTs concentrations. Hybrid

GCNTAs are also products of hydrothermal reduction of GO and CNTs. These materials can perform structural characteristics of GAs or CNTAs based on the concentrations of GO and CNTs in the initial sol suspension.

Mechanisms for the gelation process of different carbon aerogels were also covered using presented mechanisms in the literature. It is a common believe that formation of primary particle aggregates through sol-gel process results in the formation of secondary nanoparticles, which in turns can form an organic hydrogel through the aggregation process. Regarding the self-assembly process, on the other hand, it is believed that formation of π–π interactions between neighboring nanosheets during hydrothermal reduction process results in formation of elastic hydrogels.

Electrochemical and thermal properties of different types of carbon aerogels were also compared in this review. A correlation between structural characteristics and electrochemical properties of CAs was suggested in the literature. This correlation is between electrochemical parameters and crystalline structure of CAs. Consequently, one can tailor electrochemical characteristics of a carbon aerogel supercapacitor via controlling its crystalline structure. Moreover, carbon aerogels perform significant thermal resistance characteristics, even at elevated temperatures, which make them perfect candidates for thermal insulating applications at low temperatures as well as high-temperatures.

6. Outlook and future prospects

A comprehensive overview of recent advances in the carbon aerogels research area was presented in this review paper, with an emphasis on fabrication mechanisms, structural and functional properties, as well as potential application fields. Although the number of publications in the fields covered in this review paper has grown noticeably during recent years, which mostly can be attributed to the recent introduction of new self-assembled members of carbon aerogels' family (graphene- and CNT-based aerogels), but there are still numbers of unknown aspects regarding fabrication and properties of both conventional organic-based CAs and self-assembled carbon aerogels. For instance, although there are numbers of publications regarding fabrication methods for the assembly of GAs, CNTAs and nanocomposite aerogels, but the nature of gelation process of these materials through the hydrothermal reduction process is not completely discovered, and demands more efforts. The mechanism of the gelation process, including the validity of proposed cluster-aggregation nature of this process, should be confirmed. Moreover, the influences of different reducing and crosslinking agents on the hydrothermal gelation process and structural performance of fabricated gels need more investigations. These are parameters that can affect final performance of carbon aerogels in any application field.

A great progress was achieved regarding fabrication, structure and characteristics of conventional CAs, during past years. As covered in this review paper, structural characteristics and functional properties of conventional CAs have been studied in details in the literature. However, more efforts are needed to fully understand the aggregation process of cluster sub-structures, which in turns control the formation a characteristics of secondary nanoparticles in the structure o conventional CAs. In addition, novel field of carbon aeroge nanocomposite structures, which can gather interestin properties of carbon aerogels and other materials all in a singl structure, needs a great attention, as this field can provide a new path for many novel and important applications in th fascinating research area.

Acknowledgements

The authors would like to thank Tarbiat Modares University and Iran Nanotechnology Initiative Council (INIC) fo supporting this research work.

Notes and references

1. R. W. Pekala and C. T. Alviso, *MRS Proceedings*, 1992, **27**, 3-14.
2. R. W. Pekala, C. T. Alviso, F. M. Kong and S. S. Hulsey, *J. Non-Cryst. Solids*, 1992, **145**, 90-98.
3. T. Kyotani, *Carbon*, 2000, **38**, 269-286.
4. C. Moreno-Castilla and F. J. Maldonado-Hódar, *Carbon* 2005, **43**, 455-465.
5. A. M. ElKhatat and S. A. Al-Muhtaseb, *Adv. Mater.*, 2011, **23**, 2887-2903.
6. N. I. Kovtyukhova, T. E. Mallouk, L. Pan and E. C. Dickey, *Am. Chem. Soc.*, 2003, **125**, 9761-9769.
7. J. Chen, C. Xue, R. Ramasubramaniam and H. Liu, *Carbon* 2006, **44**, 2142-2146.
8. F. Liu and T. S. Seo, *Adv. Funct. Mater.*, 2010, **20**, 1930-1936.
9. Y. Xu, K. Sheng, C. Li and G. Shi, *ACS Nano*, 2010, **4**, 4324-4330.
10. Y. Xu, Q. Wu, Y. Sun, H. Bai and G. Shi, *ACS Nano*, 2010, **4**, 7358-7362.
11. H. Tamon, H. Ishizaka, M. Mikami and M. Okazaki, *Carbon*, 1997, **35**, 791-796.
12. D. Wu, R. Fu, S. Zhang, M. S. Dresselhaus and G. Dresselhaus, *J. Non-Cryst. Solids*, 2004, **336**, 26-31.
13. W. C. Li, A. H. Lu and S. C. Guo, *Carbon*, 2001, **39**, 1989-1994.
14. R. Zhang, *J. Porous Mater.*, 2003, **10**, 57-68.
15. A. Hajizadeh, A. R. Bahramian and A. Sharif, *Adv Mat Res*, 2013, **829**, 41-45.
16. I. Naseri, A. Kazemi, A. R. Bahramian and M. Razzagh Kashani, *Mater. Des.*, 2014, **61**, 35-40.
17. A. Hajizadeh, A. R. Bahramian and A. Sharif, *J. Non-Cryst Solids*, 2014, **402**, 53-57.
18. R. Zhang, Y. Lu, L. Zhan, X. Liang, G. Wu and L. Ling, *Carbon*, 2003, **41**, 1660-1663.
19. D. Wu, R. Fu, Z. Sun and Z. Yu, *J. Non-Cryst. Solids*, 2005, **351**, 915-921.
20. D. Wu and R. Fu, *J. Porous Mater.*, 2005, **12**, 311-316.
21. G. Biesmans, A. Mertens, L. Duffours, T. Woignier and Phalippou, *J. Non-Cryst. Solids*, 1998, **225**, 64-68.
22. J. Yamashita, T. Ojima, M. Shioya, H. Hatori and Y Yamada, *Carbon*, 2003, **41**, 285-294.

23. R. W. Pekala, *J Mater Sci*, 1989, **24**, 3221-3227.
24. R. Petričević, G. Reichenauer, V. Bock, A. Emmerling and J. Fricke, *J. Non-Cryst. Solids*, 1998, **225**, 41-45.
25. T. Horikawa, J. i. Hayashi and K. Muroyama, *Carbon*, 2004, **42**, 169-175.
26. N. Liu, J. Shen and D. Liu, *Microporous Mesoporous Mater.*, 2013, **167**, 176-181.
27. V. Bock, O. Nilsson, J. Blumm and J. Fricke, *J. Non-Cryst. Solids*, 1995, **185**, 233-239.
28. G. A. M. Reynolds, A. W. P. Fung, Z. H. Wang, M. S. Dresselhaus and R. W. Pekala, *J. Non-Cryst. Solids*, 1995, **188**, 27-33.
29. Y. Hanzawa, H. Hatori, N. Yoshizawa and Y. Yamada, *Carbon*, 2002, **40**, 575-581.
30. O. Czakkel, B. Nagy, E. Geissler and K. László, *J. of Supercritical Fluids*, 2013, **75**, 112-119.
31. N. Job, R. Pirard, J. Marien and J.-P. Pirard, *Carbon*, 2004, **42**, 619-628.
32. R. W. Pekala, C. T. Alviso and J. D. LeMay, *J. Non-Cryst. Solids*, 1990, **125**, 67-75.
33. H. Tamon, H. Ishizaka, T. Araki and M. Okazaki, *Carbon*, 1998, **36**, 1257-1262.
34. V. Bock, A. Emmerling and J. Fricke, *J. Non-Cryst. Solids*, 1998, **225**, 69-73.
35. N. Job, A. Théry, R. Pirard, J. Marien, L. Kocon, J.-N. Rouzaud, F. Béguin and J.-P. Pirard, *Carbon*, 2005, **43**, 2481-2494.
36. D. F. Albert, G. R. Andrews, R. S. Mendenhall and J. W. Bruno, *J. Non-Cryst. Solids*, 2001, **296**, 1-9.
37. Z. T. Mazraeh-shahi, A. M. Shoushtari, M. Abdouss and A. R. Bahramian, *J. Non-Cryst. Solids*, 2013, **376**, 30-37.
38. O. Czakkel, K. Marthi, E. Geissler and K. László, *Microporous Mesoporous Mater.*, 2005, **86**, 124-133.
39. R. W. Pekala, C. T. Alviso, X. Lu, J. Gross and J. Fricke, *J. Non-Cryst. Solids*, 1995, **188**, 34-40.
40. H. Tamon and H. Ishizaka, *Carbon*, 1998, **36**, 1397-1399.
41. B. Mathieu, S. Blacher, R. Pirard, J. P. Pirard, B. Sahouli and F. Brouers, *J. Non-Cryst. Solids*, 1997, **212**, 250-261.
42. H. Tamon, H. Ishizaka, T. Yamamoto and T. Suzuki, *Carbon*, 2000, **38**, 1099-1105.
43. T. Yamamoto, T. Nishimura, T. Suzuki and H. Tamon, *J. Non-Cryst. Solids*, 2001, **288**, 46-55.
44. D. Wu, R. Fu and Z. Yu, *J. Appl. Polym. Sci.*, 2005, **96**, 1429-1435.
45. R. W. Pekala and D. W. Schaefer, *Macromolecules*, 1993, **26**, 5487-5493.
46. T. Horikawa, J. i. Hayashi and K. Muroyama, *Carbon*, 2004, **42**, 1625-1633.
47. W. C. Li, A. H. Lu and F. Schüth, *Chem. Mater.*, 2005, **17**, 3620-3626.
48. D. Wu, R. Fu, S. Zhang, M. S. Dresselhaus and G. Dresselhaus, *Carbon*, 2004, **42**, 2033-2039.
49. R. Fu, B. Zheng, J. Liu, M. S. Dresselhaus, G. Dresselhaus, J. H. Satcher and T. F. Baumann, *Adv. Funct. Mater.*, 2003, **13**, 558-562.
50. T. F. Baumann, M. A. Worsley, T. Y.-J. Han and J. H. Satcher, *J. Non-Cryst. Solids*, 2008, **354**, 3513-3515.
51. D. Fairén-Jiménez, F. Carrasco-Marín and C. Moreno-Castilla, *Carbon*, 2006, **44**, 2301-2307.
52. M. Mirzaeian and P. J. Hall, *Electrochim. Acta*, 2009, **54**, 7444-7451.
53. X.-L. Wu, T. Wen, H.-L. Guo, S. Yang, X. Wang and A.-W. Xu, *ACS Nano*, 2013, **7**, 3589-3597.
54. F. J. Maldonado-Hódar, M. A. Ferro-García, J. Rivera-Utrilla and C. Moreno-Castilla, *Carbon*, 1999, **37**, 1199-1205.
55. M. B. Bryning, D. E. Milkie, M. F. Islam, L. A. Hough, J. M. Kikkawa and A. G. Yodh, *Adv. Mater.*, 2007, **19**, 661-664.
56. M. C. Gutierrez, M. J. Hortiguela, J. M. Amarilla, F. Jimenez, M. L. Ferrer and F. delMonte, *J. Phys. Chem. C*, 2007, **111**, 5557-5560.
57. J. Zou, L. Liu, H. Chen, S. I. Khondaker, R. D. McCullough, Q. Huo and L. Zhai, *Adv. Mater.*, 2008, **20**, 2055-2060.
58. J. Zou, S. I. Khondaker, Q. Huo and L. Zhai, *Adv. Funct. Mater.*, 2009, **19**, 479-483.
59. R. R. Kohlmeyer, M. Lor, J. Deng, H. Liu and J. Chen, *Carbon*, 2011, **49**, 2352-2361.
60. S.-M. Kwon, H.-S. Kim and H.-J. Jin, *Polymer*, 2009, **50**, 2786-2792.
61. G. N. Ostojic, *ChemPhysChem*, 2012, **13**, 2102-2107.
62. J. Zou, J. Liu, A. S. Karakoti, A. Kumar, D. Joung, Q. Li, S. I. Khondaker, S. Seal and L. Zhai, *ACS Nano*, 2010, **4**, 7293-7302.
63. A. Allahbakhsh, F. Sharif and S. Mazinani, *Nano*, 2013, **8**, 1350045.
64. X. Wu, J. Zhou, W. Xing, G. Wang, H. Cui, S. Zhuo, Q. Xue, Z. Yan and S. Z. Qiao, *J. Mater. Chem.*, 2012, **22**, 23186.
65. Y. Lin, G. J. Ehlert, C. Bukowsky and H. A. Sodano, *ACS Appl. Mater. Interfaces*, 2011, **3**, 2200-2203.
66. X. Mi, G. Huang, W. Xie, W. Wang, Y. Liu and J. Gao, *Carbon*, 2012, **50**, 4856-4864.
67. S. T. Nguyen, H. T. Nguyen, A. Rinaldi, N. P. V. Nguyen, Z. Fan and H. M. Duong, *Colloids and Surfaces A Physicochem. Eng. Aspects*, 2012, **414**, 352-358.
68. X. Zhang, Z. Sui, B. Xu, S. Yue, Y. Luo, W. Zhan and B. Liu, *J. Mater. Chem.*, 2011, **21**, 6494.
69. Z. Sui, X. Zhang, Y. Lei and Y. Luo, *Carbon*, 2011, **49**, 4314-4321.
70. Z. Fan, D. Z. Y. Tng, S. T. Nguyen, J. Feng, C. Lin, P. Xiao, J. Lu and H. M. Duong, *Chem. Phys. Lett.*, 2013, **561-562**, 92-96.
71. W. Chen and L. Yan, *Nanoscale*, 2011, **3**, 3132.
72. W. Chen, S. Li, C. Chen and L. Yan, *Adv. Mater.*, 2011, **23**, 5679-5683.
73. H. D. Pham, V. H. Pham, T. V. Cuong, T.-D. Nguyen-Phan, J. S. Chung, E. W. Shin and S. Kim, *Chem. Commun.*, 2011, **47**, 9672.
74. H. Bai, C. Li, X. Wang and G. Shi, *J. Phys. Chem. C*, 2011, **115**, 5545-5551.
75. J. Wang, Z. Shi, J. Fan, Y. Ge, J. Yin and G. Hu, *J. Mater. Chem.*, 2012, **22**, 22459.
76. C.-C. Ji, M.-W. Xu, S.-J. Bao, C.-J. Cai, Z.-J. Lu, H. Chai, F. Yang and H. Wei, *J. Colloid Interface Sci.*, 2013, **407**, 416-424.
77. M. A. Worsley, P. J. Pauzauskie, T. Y. Olson, J. Biener, J. H. Satcher and T. F. Baumann, *J. Am. Chem. Soc.*, 2010, **132**, 14067-14069.
78. F. Meng, X. Zhang, B. Xu, S. Yue, H. Guo and Y. Luo, *J. Mater. Chem.*, 2011, **21**, 18537.
79. M. A. Worsley, T. Y. Olson, J. R. I. Lee, T. M. Willey, M. H. Nielsen, S. K. Roberts, P. J. Pauzauskie, J. Biener, J. H. Satcher and T. F. Baumann, *J. Phys. Chem. Lett.*, 2011, **2**, 921-925.

80. K. Zhang, B. T. Ang, L. L. Zhang, X. S. Zhao and J. Wu, *J. Mater. Chem.*, 2011, **21**, 2663.
81. Z. M. Marković, B. M. Babić, M. D. Dramićanin, I. D. Holclajtner Antunović, V. B. Pavlović, D. B. Peruško and B. M. Todorović Marković, *Synth. Met.*, 2012, **162**, 743-747.
82. K. Guo, H. Song, X. Chen, X. Du and L. Zhong, *PCCP*, 2014, **16**, 11603.
83. Y. J. Lee, H. W. Park, G.-P. Kim, J. Yi and I. K. Song, *Curr. Appl Phys.*, 2013, **13**, 945-949.
84. Z.-Y. Sui, Y. Cui, J.-H. Zhu and B.-H. Han, *ACS Appl. Mater. Interfaces*, 2013, **5**, 9172-9179.
85. L. Liu, J. Yang and Q. Meng, *J. Sol-Gel Sci. Technol.*, 2013, **66**, 1-5.
86. Y. Qian, I. M. Ismail and A. Stein, *Carbon*, 2014, **68**, 221-231.
87. Y. Zhang, W. Fan, Y. Huang, C. Zhang and T. Liu, *RSC Adv.*, 2015, **5**, 1301-1308.
88. H. Hu, Z. Zhao, W. Wan, Y. Gogotsi and J. Qiu, *ACS Appl. Mater. Interfaces*, 2014, **6**, 3242-3249.
89. J. L. Vickery, A. J. Patil and S. Mann, *Adv. Mater.*, 2009, **21**, 2180-2184.
90. M. A. Worsley, P. J. Pauzauskie, S. O. Kucheyev, J. M. Zaug, A. V. Hamza, J. H. Satcher and T. F. Baumann, *Acta Mater.*, 2009, **57**, 5131-5136.
91. M. Haghgoo, A. A. Yousefi, M. J. Zohouriaan Mehr, A. Celzard, V. Fierro, A. Léonard and N. Job, *Microporous Mesoporous Mater.*, 2014, **184**, 97-104.
92. K. H. Kim, M. Vural and M. F. Islam, *Adv. Mater.*, 2011, **23**, 2865-2869.
93. S. Kabiri, D. N. H. Tran, T. Altalhi and D. Losic, *Carbon*, 2014, **80**, 523-533.
94. Z. Fan, D. Z. Y. Tng, C. X. T. Lim, P. Liu, S. T. Nguyen, P. Xiao, A. Marconnet, C. Y. H. Lim and H. M. Duong, *Colloids and Surfaces A: Physicochem. Eng. Aspects*, 2014, **445**, 48-53.
95. F. Zhang, J. Tang, Z. Wang and L.-C. Qin, *Chem. Phys. Lett.*, 2013, **590**, 121-125.
96. S. J. Taylor, M. D. Haw, J. Sefcik and A. J. Fletcher, *Langmuir*, 2014, **30**, 10231-10240.
97. V. G. Pol, L. K. Shrestha and K. Ariga, *ACS Appl. Mater. Interfaces*, 2014, **6**, 10649-10655.
98. H. Tamon and H. Ishizaka, *J. Colloid Interface Sci.*, 1998, **206**, 577-582.
99. D. Long, R. Zhang, W. Qiao, L. Zhang, X. Liang and L. Ling, *J. Colloid Interface Sci.*, 2009, **331**, 40-46.
100. N. Liu, S. Zhang, R. Fu, M. S. Dresselhaus and G. Dresselhaus, *J. Appl. Polym. Sci.*, 2007, **104**, 2849-2855.
101. L. Weigold, D. P. Mohite, S. Mahadik-Khanolkar, N. Leventis and G. Reichenauer, *J. Non-Cryst. Solids*, 2013, **368**, 105-111.
102. D. Wu, R. Fu, M. S. Dresselhaus and G. Dresselhaus, *Carbon*, 2006, **44**, 675-681.
103. N. Tonanon, W. Tanthapanichakoon, T. Yamamoto, H. Nishihara, S. R. Mukai and H. Tamon, *Carbon*, 2003, **41**, 2981-2990.
104. J. Li, X. Wang, Q. Huang, S. Gamboa and P. J. Sebastian, *J. Power Sources*, 2006, **158**, 784-788.
105. A. Hajizadeh, A. R. Bahramian, A. Seifi and I. Naseri, *J. Sol-Gel Sci. Technol.*, 2014, **73**, 220-226.
106. C. Lin and J. A. Ritter, *Carbon*, 1997, **35**, 1271-1278.
107. N. Job, F. Panariello, M. Crine, J.-P. Pirard and A. Léonard, *Colloids and Surfaces A: Physicochem. Eng. Aspects*, 2007, **293**, 224-228.
108. J. Gross, G. W. Scherer, C. T. Alviso and R. W. Pekala, *J. Non-Cryst. Solids*, 1997, **211**, 132-142.
109. I. Naseri, A. Kazemi, A. R. Bahramian and M. R. Kashani, *Adv Mat Res*, 2013, **829**, 182-186.
110. E. Gallegos-Suárez, A. F. Pérez-Cadenas, F. J. Maldonado-Hódar and F. Carrasco-Marín, *Chem. Eng. J.*, 2012, **181-182**, 851-855.
111. M. Mirzaeian and P. J. Hall, *J Mater Sci*, 2009, **44**, 2705-2713.
112. D. W. Schaefer, R. Pekala and G. Beaucage, *J. Non-Cryst. Solids*, 1995, **186**, 159-167.
113. J. Feng, J. Feng and C. Zhang, *J. Sol-Gel Sci. Technol.*, 2011, **59**, 371-380.
114. A. Szczurek, G. Amaral-Labat, V. Fierro, A. Pizzi, E. Masson and A. Celzard, *Mater. Chem. Phys.*, 2011, **129**, 1221-1232.
115. H. Tamon, H. Ishizaka, T. Yamamoto and T. Suzuki, *Carbon*, 1999, **37**, 2049-2055.
116. R. Kocklenberg, B. Mathieu, S. Blacher, R. Pirard, J. P. Pirard, R. Sobry and G. Van den Bossche, *J. Non-Cryst. Solids*, 1998, **225**, 8-13.
117. K.-x. Sheng, Y.-x. Xu, C. Li and G.-q. Shi, *New Carbon Mater.*, 2011, **26**, 9-15.
118. J. Li, J. Li, H. Meng, S. Xie, B. Zhang, L. Li, H. Ma, J. Zhang and M. Yu, *J. Mater. Chem. A*, 2014, **2**, 2934.
119. J. Liang, Z. Cai, L. Li, L. Guo and J. Geng, *RSC Adv.*, 2014, **4**, 4843.
120. Q. Shao, J. Tang, Y. Lin, J. Li, F. Qin, J. Yuan and L.-C. Qin, *J. Power Sources*, 2015, **278**, 751-759.
121. J.-Y. Hong, E.-H. Sohn, S. Park and H. S. Park, *Chem. Eng. J.*, 2015, **269**, 229-235.
122. H. Sun, Z. Xu and C. Gao, *Adv. Mater.*, 2013, **25**, 2554-2560.
123. A. K. Meena, G. K. Mishra, P. K. Rai, C. Rajagopal and P. N. Nagar, *J. Hazard. Mater.*, 2005, **122**, 161-170.
124. G. Wei, Y.-E. Miao, C. Zhang, Z. Yang, Z. Liu, W. W. Tjiu and T. Liu, *ACS Appl. Mater. Interfaces*, 2013, **5**, 7584-7591.
125. J. Feng, C. Zhang, J. Feng, Y. Jiang and N. Zhao, *ACS Appl. Mater. Interfaces*, 2011, **3**, 4796-4803.
126. G. M. Pajonk, A. V. Rao, N. Pinto, F. Ehrburger-Dolle and M. B. Gil, 1998, **118**, 167-174.
127. R. W. Pekala, J. C. Farmer, C. T. Alviso, T. D. Tran, S. T. Mayer, J. M. Miller and B. Dunn, *J. Non-Cryst. Solids*, 1995, **225**, 74-80.
128. J. Wang, L. Angnes, H. Tobias, R. A. Roesner, K. C. Hong, P. S. Glass, F. M. Kong and R. W. Pekala, *Anal. Chem.*, 1993, **65**, 2300-2303.
129. T. Tsuchiya, T. Mori, S. Iwamura, I. Ogino and S. R. Mukai, *Carbon*, 2014, **76**, 240-249.
130. S.-W. Hwang and S.-H. Hyun, *J. Non-Cryst. Solids*, 2004, **347**, 238-245.
131. S. J. Kim, S. W. Hwang and S. H. Hyun, *J Mater Sci*, 2005, **40**, 725-731.
132. R. Saliger, V. Bock, R. Petricevic, T. Tillotson, S. Geis and J. Fricke, *J. Non-Cryst. Solids*, 1997, **221**, 144-150.
133. G.-P. Hao, F. Han, D.-C. Guo, R.-J. Fan, G. Xiong, W.-C. Li and A.-H. Lu, *J. Phys. Chem. C*, 2012, **116**, 10303-10311.
134. W. Si, X. Wu, J. Zhou, F. Guo, S. Zhuo, H. Cui and W. Xing, *Nanoscale Res. Lett.*, 2013, **8**, 247.

135. L. Chen, M. Feng and H. Zhan, *RSC Adv.*, 2014, **4**, 30689.
136. G. Tang, Z.-G. Jiang, X. Li, H.-B. Zhang, A. Dasari and Z.-Z. Yu, *Carbon*, 2014, **77**, 592-599.
137. X. Lu, O. Nilsson, J. Fricke and R. W. Pekala, *J. Appl. Phys.*, 1993, **73**, 581.
138. M. Wiener, G. Reichenauer, S. Braxmeier, F. Hemberger and H. P. Ebert, *Int. J. Thermophys.*, 2009, **30**, 1372-1385.
139. M. Wiener, G. Reichenauer, F. Hemberger and H. P. Ebert, *Int. J. Thermophys.*, 2006, **27**, 1826-1843.
140. J. Feng, J. Feng, Y. Jiang and C. Zhang, *Mater. Lett.*, 2011, **65**, 3454-3456.
141. L. W. Hrubesh and R. W. Pekala, *J. Mater. Res.*, 1994, **9**, 731-738.
142. J. Feng, J. Feng and C. Zhang, *J. Porous Mater.*, 2011, **19**, 551-556.
143. Z. Fan, A. Marconnet, S. T. Nguyen, C. Y. H. Lim and H. M. Duong, *Int. J. Heat Mass Transfer*, 2014, **76**, 122-127.
144. A. Smirnova, X. Dong, H. Hara, A. Vasiliev and N. Sammes, *Int. J. Hydrogen Energy*, 2005, **30**, 149-158.
145. D. Ábrahám, B. Nagy, G. Dobos, J. Madarász, G. Onyestyák, M. V. Trenikhin and K. László, *Microporous Mesoporous Mater.*, 2014, **190**, 46-53.
146. E. Guilminot, F. Fischer, M. Chatenet, A. Rigacci, S. Berthon-Fabry, P. Achard and E. Chainet, *J. Power Sources*, 2007, **166**, 104-111.
147. R. Du, N. Zhang, J. Zhu, Y. Wang, C. Xu, Y. Hu, N. Mao, H. Xu, W. Duan, L. Zhuang, L. Qu, Y. Hou and J. Zhang, *Small*, 2015, DOI: 10.1002/smll.201500587, n/a-n/a.
148. H. Li, X. Gui, C. Ji, P. Li, Z. Li, L. Zhang, E. Shi, K. Zhu, J. Wei, K. Wang, H. Zhu, D. Wu and A. Cao, *Nano Research*, 2012, **5**, 265-271.
149. H. Yin, C. Zhang, F. Liu and Y. Hou, *Adv. Funct. Mater.*, 2014, **24**, 2930-2937.
150. Z.-S. Wu, S. Yang, Y. Sun, K. Parvez, X. Feng and K. Müllen, *J. Am. Chem. Soc.*, 2012, **134**, 9082-9085.
151. X. Jiang, X. Yang, Y. Zhu, J. Shen, K. Fan and C. Li, *J. Power Sources*, 2013, **237**, 178-186.
152. B. Qiu, M. Xing and J. Zhang, *J. Am. Chem. Soc.*, 2014, **136**, 5852-5855.
153. P. Huang, W. Chen and L. Yan, *Nanoscale*, 2013, **5**, 6034.
154. H. Kabbour, T. F. Baumann, J. H. Satcher, A. Saulnier and C. C. Ahn, *Chem. Mater.*, 2006, **18**, 6085-6087.
155. Z.-Y. Wu, C. Li, H.-W. Liang, J.-F. Chen and S.-H. Yu, *Angew. Chem.*, 2013, **125**, 2997-3001.
156. Y.-Q. Li, Y. A. Samad, K. Polychronopoulou, S. M. Alhassan and K. Liao, *ACS Sustainable Chem. Eng.*, 2014, **2**, 1492-1497.